SSCL-346

SSCL-346

Superconducting Super Collider Laboratory

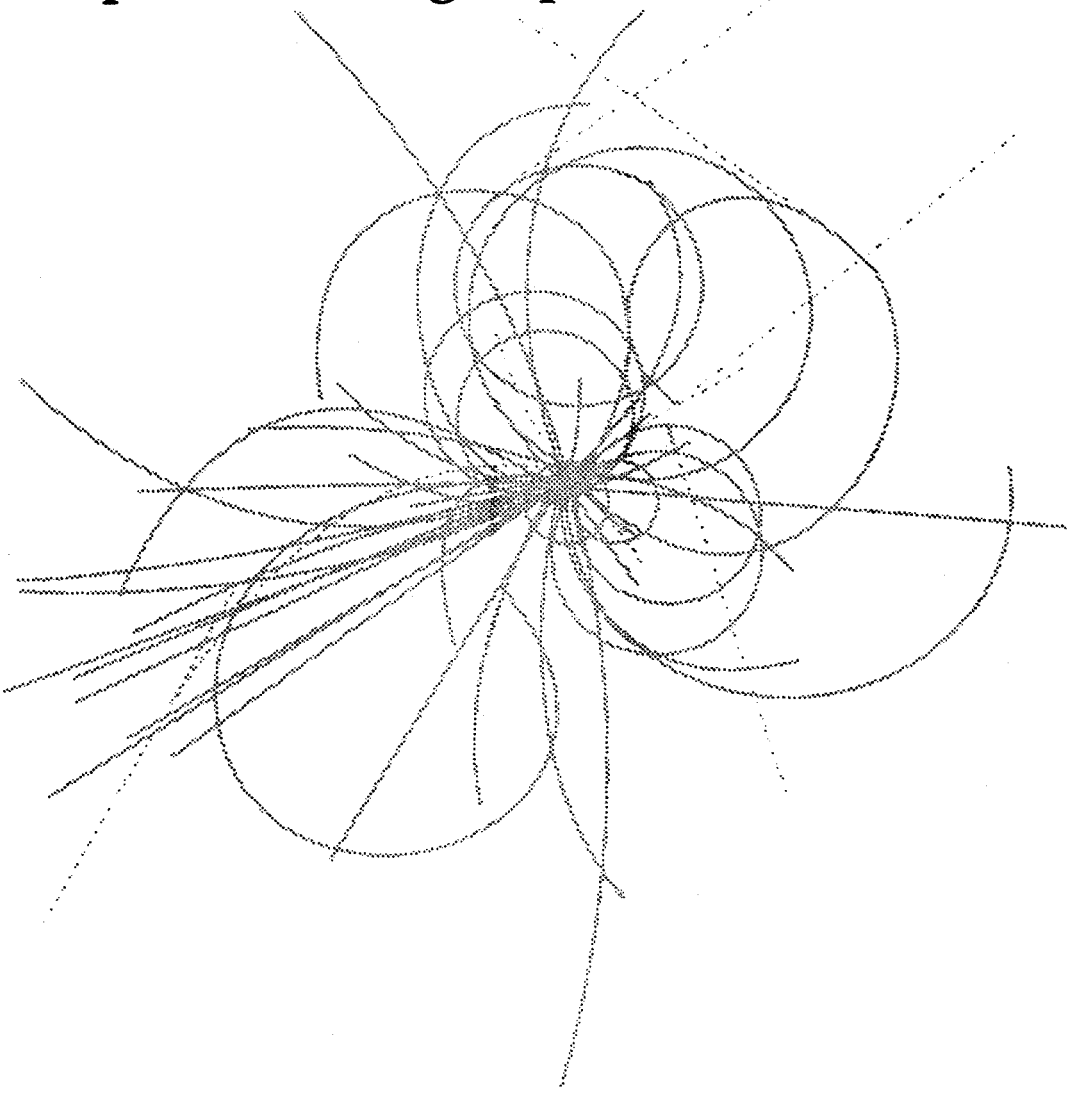

Coherent Beam-Beam Effects

A Chao

January 1991

SSCL-346

COHERENT BEAM-BEAM EFFECTS

Alexander W. Chao

Accelerator Division
Superconducting Super Collider Laboratory*
2550 Beckleymeade Avenue
Dallas, TX 75237

January 1991

* Operated by the Universities Research Association, Inc., for the U.S. Department of Energy under Contract No. DE-AC02-89ER40486.

TABLE OF CONTENTS

1.0 INTRODUCTION 1

2.0 THE DYNAMIC-BETA MODEL 2

3.0 FLIP-FLOP EFFECT 6

4.0 STEADY-STATE WITH NONLINEAR BEAM-BEAM FORCE 7

5.0 DYNAMICS ABOUT THE STEADY-STATE 10

6.0 RIGID DIPOLE MODEL 11

- 6.1 Unequal Beams 17
- 6.2 Unequal Tunes 18
- 6.3 Phase Advance Errors 18
- 6.4 Unequal Circumferences 19
- 6.5 Four Beam Compensation 21
- 6.6 Synchro-betatron Resonances 24
- 6.7 Spontaneous Beam Separation 24

7.0 QUADRUPOLE MODES 28

8.0 QUADRUPOLE MODES AROUND DYNAMIC-BETA 30

- 8.1 The First Model 30
- 8.2 The Second Model 35

9.0 HIGHER ORDER MOMENTS 37

10.0 COHERENT BEAM BLOW-UP MODEL 41

REFERENCES 45

1.0 INTRODUCTION

There are two physical pictures that describe the beam-beam interaction in a storage ring collider: the weak-strong and the strong-strong pictures as shown in Figure 1. Both pictures play a role in determining the beam-beam behavior. This review addresses only the strong-strong picture. The corresponding beam dynamical effects are referred to as the coherent beam-beam effects. Some basic knowledge of the weak-strong picture is assumed.[1] To be specific, two beams of opposite charges are considered.

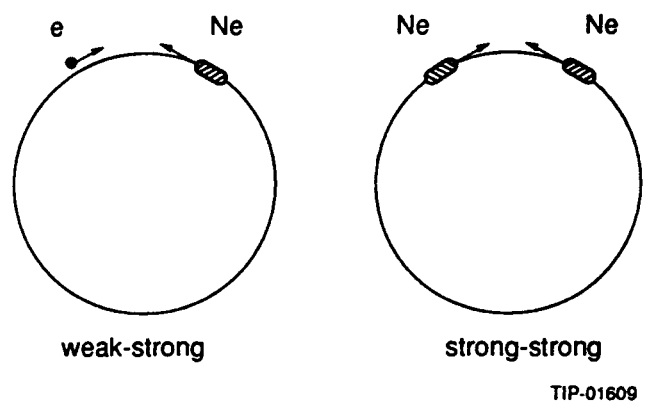

Figure 1. Weak-strong and Strong-strong Beam-beam Interaction.

In the weak-strong picture, the strong beam is unperturbed by the weak beam. It is regarded as a rigid nonlinear lens at the beam-beam interaction points (IP). Beam dynamics in this picture is that of an incoherent single-particle motion in the presence of a static nonlinear lens. The beam-beam problem is reduced to a nonlinear mapping problem.

In the strong-strong picture, both beams are perturbed. To study the coherent beam-beam effects, the procedure in principle is as follows:

(a) Let the steady-state distribution be Ψ_0. For example, Ψ_0 may be gaussian in the absence of the beam-beam interaction. With strong-strong perturbation, Ψ_0 must be solved in a self-consistent manner and in general is no longer gaussian.

(b) Given the perturbed, generally non-gaussian Ψ_0, consider distributions of the $\pm$ beams that deviate from Ψ_0, i.e.,

$$\begin{aligned} \Psi_+ &= \Psi_0 + \Delta\Psi_+ \\ \Psi_- &= \Psi_0 + \Delta\Psi_- \ . \end{aligned} \tag{1}$$

The + beam sees the beam-beam force from the − beam, which is related to Ψ_-, while the − beam sees a beam-beam force similarly related to Ψ_+. The beam-beam force thus provides the coupling between $\Delta\Psi_\pm$. The question is then: are infinitesimal perturbations $\Delta\Psi_\pm$ stable under their mutual interaction? Stability of $\Delta\Psi_\pm$ determines the stability of the beam-beam system.

However, neither of the above steps is straightforward. Although much progress has been made, studies on coherent beam-beam effects so far have covered only pieces of the complex problem. This paper is a summary of some of these studies.

2.0 THE DYNAMIC-BETA MODEL

This is the simplest model in the strong-strong picture.[2] To proceed, consider a linearized beam-beam force (linearized with respect to the coordinates x and y of the particle which is experiencing the force). In this case, the perturbed steady-state Ψ_0 is gaussian if the unperturbed one is gaussian. The linear beam-beam force of one beam perturbs the other beam in such a way that the betatron phase advance between IPs $\mu_{x0,y0}$, the beta-functions at the IPs $\beta^*{}_{x0,y0}$, and the rms beam sizes at the IPs $\sigma_{x0,y0}$ are perturbed to become $\mu_{x,y}$, $\beta^*{}_{x,y}$, and $\sigma_{x,y}$ respectively. The perturbed quantities are given by

$$\cos\mu_{x,y} = \cos\mu_{x0,y0} - 2\pi\zeta_{x,y}\sin\mu_{x0,y0} \tag{2a}$$

$$\beta^*{}_{x0,y0}/\beta^*{}_{x,y} = \sin\mu_{x,y}/\sin\mu_{x0,y0} \tag{2b}$$

where $\zeta_{x,y}$ is the beam-beam strength parameter

$$\zeta_{x,y} = N\, r_0\, \beta^*{}_{x0,y0}/2\pi\gamma\sigma_{x,y}\,(\sigma_x + \sigma_y) \tag{3}$$

with γ the relativistic factor, N the number of particles-per-beam bunch, and $r_0 = e^2/mc^2$ the classical radius of the particle. Note that it is the unperturbed beta-functions and the perturbed beam sizes that appear in the expression of $\zeta_{x,y}$, Eq. (3).

Stability of the beams under linearized perturbations requires $|\cos\mu_{x,y}| \leq 1$. This means, using Eq. (2a) and dropping subscripts x and y for abbreviation,

$$\zeta \leq \cot(\mu_0/2)/2\pi\,. \tag{4}$$

Figure 2 shows the region of stability in the (ζ, ν_0) space, where ν_0, defined as $\mu_0/2\pi$, is the tune advance between IPs. The diagram repeats with a period of $\nu_0 = 1/2$. Sometimes, it is referred to as the sawtooth diagram because of its appearance when illustrated with

a wider range of ν_0. Note that when ν_0 is close to but slightly below a multiple of 1/2, the stability region shrinks to zero. In other words, near 1/2-integer resonances, when $\nu_0 = m/2$, even a weak beam-beam perturbation makes the beam unstable.

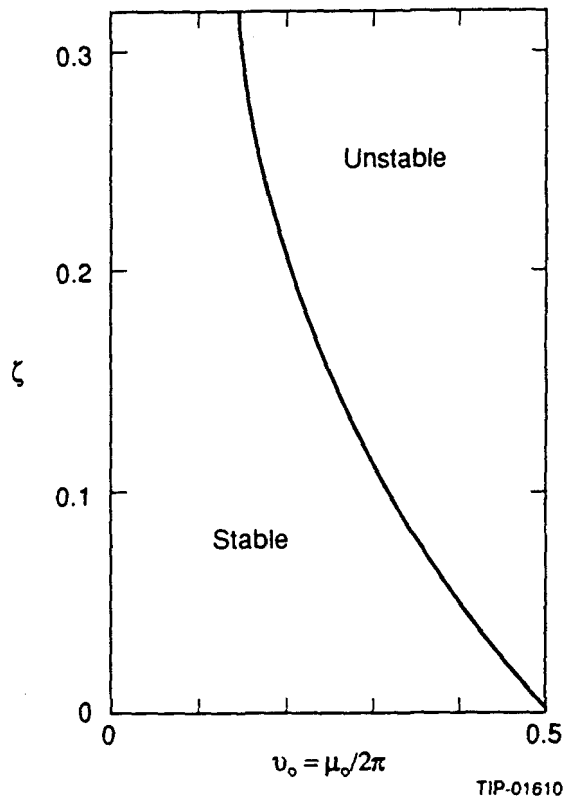

Figure 2. Stability Diagram of the Dynamic-beta Effect. The incoherent weak-strong case has the same diagram if ζ is replaced by ζ_0. The behavior repeats with period $\nu_0 = 1/2$.

In the incoherent case, the weak beam is perturbed by the strong beam. If the beam-beam force is linearized, the perturbed quantities of the weak beam are also given by Eq. (2), except that the beam-beam strength parameter $\zeta_{x,y}$ is given by the strong-beam values which are always unperturbed. The incoherent stability condition is

$$\zeta_0 \leq \cot(\mu_0/2)/2\pi. \tag{5}$$

Although similar, Eqs. (4) and (5) have very different contents. In particular, Eq. (5) can be violated if one increases the beam intensity N, but it will be shown later that Eq. (4) is always satisfied for any value of N.

In solving Eqs. (2) and (3) for the strong-strong case, we note that the perturbed beam sizes scale with the perturbed beta-functions (the dynamic-beta), i.e., $\sigma_{x,y} \propto \sqrt{\beta^*{}_{x,y}}$, not $\sqrt{\beta^*{}_{x0,y0}}$, assuming beam emittances are unchanged due to beam-beam interaction. Further noting that $\beta^*{}_{x,y}$ depend on the perturbed beam-beam parameters $\zeta_{x,y}$, which in turn depend on $\sigma_{x,y}$, we conclude that $\sigma_{x,y}$, $\beta^*{}_{x,y}$, $\mu_{x,y}$, $\zeta_{x,y}$ and luminosity L need to be found self-consistently for a given value of N. The luminosity is given by

$$L = N^2 f M / 4\pi\sigma_x\sigma_y \tag{6}$$

where f is the revolution frequency of the beams around the storage ring, and M is the number of bunches in each beam.

As an example, consider the case of round beams $\sigma_{x0} = \sigma_{y0} = \sigma_0$ and $\mu_{x0} = \mu_{y0} = \mu_0$. Squaring both sides of Eq. (2b) and eliminating $\sin^2\mu_{x,y}$ using Eq. (2a) give a self-consistency expression for $\beta^*/\beta^*{}_0$:

$$\left(\frac{\beta^*{}_0}{\beta^*}\right)^2 = 1 + 2\rho_0 \cot\mu_0 \frac{\beta^*{}_0}{\beta^*} - \rho_0{}^2 \left(\frac{\beta^*{}_0}{\beta^*}\right)^2 \tag{7}$$

where $\rho_0 = 2\pi\zeta_0$ has been defined. Beam intensity N is contained in ρ_0.

Equation (7) can be solved to give $\beta^*/\beta^*{}_0$ in terms of the unperturbed quantities:

$$\frac{\beta^*}{\beta^*{}_0} = \sqrt{1 + \left(\frac{\rho_0}{\sin\mu_0}\right)^2} - \rho_0 \cot\mu_0 \ . \tag{8}$$

Ratios of other quantities follow from Eq. (8):

$$\frac{\beta^*{}_0}{\beta^*} = \frac{\zeta}{\zeta_0} = \frac{\sigma_0{}^2}{\sigma^2} = \frac{L}{L_0} \ . \tag{9}$$

Figure 3 shows the dependences of the dynamic-beta, the perturbed beam-beam parameter, and the luminosity on beam intensity N for various values of ν_0. As far as the dynamic-beta effect is concerned, the luminosity would benefit from having ν_0 slightly above a 1/2-integer and would suffer if it is slightly below a 1/2-integer.

As N increases, the beam-beam parameter approaches a constant value from below as shown in Figure 3(b). The constant value is that of the stability condition, Eq. (4). This means that for round beams, $\zeta \rightarrow$ constant, $\sigma \rightarrow \sqrt{N}$, and $L \rightarrow N$ as $N \rightarrow \infty$, to be

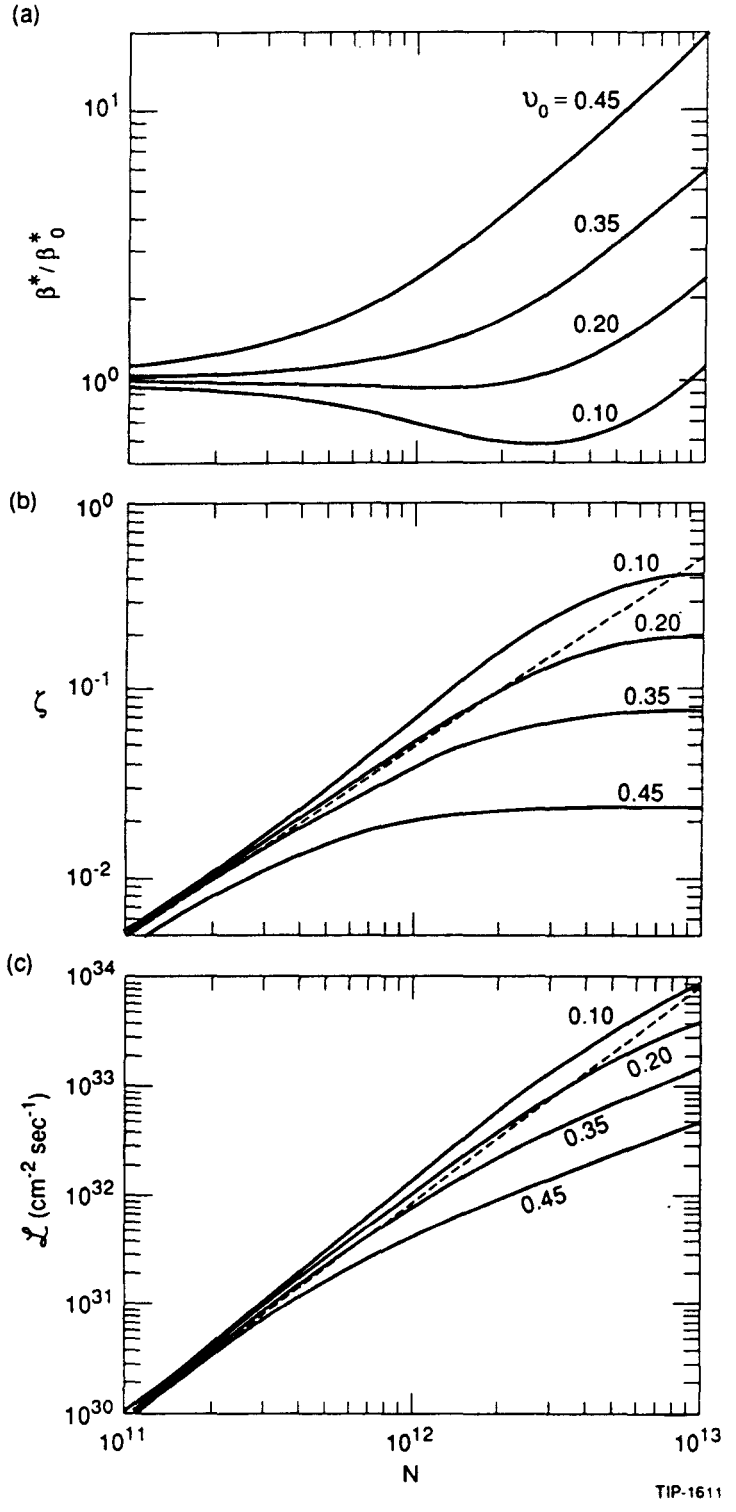

Figure 3. Dynamic-beta Behavior of β^*/β^*_0, ζ and L as Functions of N for Various Values of ν_0 (the Unperturbed Tune Advance between IPs, Modulus 1/2). Dashed curves in (b) and (c) are the unperturbed case. Numbers are normalized so that $L_0 = 10^{32}\,\mathrm{cm}^{-2}\mathrm{s}^{-1}$, $\rho_0 = 0.05$ when $N = 10^{12}$.

compared with the weak-strong case which predicts $\zeta \to N$, $\sigma \to$ constant, and $L \to N^2$ as $N \to \infty$. More significantly, this means that as N is increased, the beam size always expands sufficiently to avoid violating the instability condition (4). The two beams are always stable.

Although the system is always stable, it still suffers from resonances. The beams blow up and L levels off faster when ν_0 is just below an 1/2-integer.

Figure 3 is true for a round beam. In case of a flat beam, a different scaling is obtained with N. As $N \to \infty$, dynamic-beta model gives $\zeta_x \to N$ (provided it stays well below the instability condition), $\sigma_x \to$ constant, $\zeta_y \to$ constant, $\sigma_y \to N$, and $L \to N$. Compare with Figure 26 later.

3.0 FLIP-FLOP EFFECT

The dynamic-beta model discussed in the previous section can be generalized. Still consider round beams and linearized beam-beam forces, but now allow the two beams to behave differently. Using a similar derivation to Eq. (7) but keeping track of the fact that the perturbation of one beam is due to the beam-beam force from the other beam, we obtain (let $\rho_{o+} = \rho_{o-} = \rho_0$)

$$\begin{aligned}\left(\frac{\beta^*{}_0}{\beta^*{}_+}\right)^2 &= 1 + 2\rho_0 \cot \mu_0 \frac{\beta^*{}_0}{\beta^*{}_-} - \rho_0{}^2 \left(\frac{\beta^*{}_0}{\beta^*{}_-}\right)^2 \\ \left(\frac{\beta^*{}_0}{\beta^*{}_-}\right)^2 &= 1 + 2\rho_0 \cot \mu_0 \frac{\beta^*{}_0}{\beta^*{}_+} - \rho_0{}^2 \left(\frac{\beta^*{}_0}{\beta^*{}_+}\right)^2 .\end{aligned} \tag{10}$$

One obvious solution is $\beta^*{}_+ = \beta^*{}_-$, i.e., Eq. (7). The other set of solutions with $\beta^*{}_+ \neq \beta^*{}_-$ is found to be

$$\frac{\beta^*{}_0}{\beta^*{}_\pm} = \frac{1}{\rho_0{}^2 - 1} \left\{ \rho_0 \cot \mu_0 \pm \sqrt{\frac{\rho_0{}^2 \cot^2 \mu_0 \left(\rho_0{}^2 - 3\right) + \left(\rho_0{}^2 - 1\right)^2}{\rho_0{}^2 + 1}} \right\} . \tag{11}$$

In case the beams remain in this solution, one beam is statically blown up ($\beta^*{}_+$), while the other pinches ($\beta^*{}_-$). Equation (11) constitutes a bi-stable state of the beams because switching the roles of the blown-up beam and the pinched beam is also a solution. This situation can be a model for the "flip-flop" phenomenon[3–6] observed in storage ring colliders. Note that this is only the simplest possible explanation of the flip-flop effect. Another possibility will be mentioned later.

Figure 4 shows the steady-state dynamic-beta solutions as functions of ρ_0. The equal-beam solution (8) always exists for all values of ρ_0. The flip-flop solution (11) exists only over a finite range of ρ_0:

$$\cot\frac{\mu_0}{2} > \rho_0 > \sqrt{1+\frac{\cos^2\mu_0+\sqrt{\cos^4\mu_0+8\cos^2\mu_0}}{2}}\,. \tag{12}$$

At the lower end of the range, the equal-beam and the flip-flop solutions coincide. At the higher end, the blown-up beam in the flip-flop solution has infinite beam size. The pinched beam in this case sees no beam-beam force from the blown-up beam, and its beam size is unperturbed, i.e., $\sigma_- = \sigma_0$.

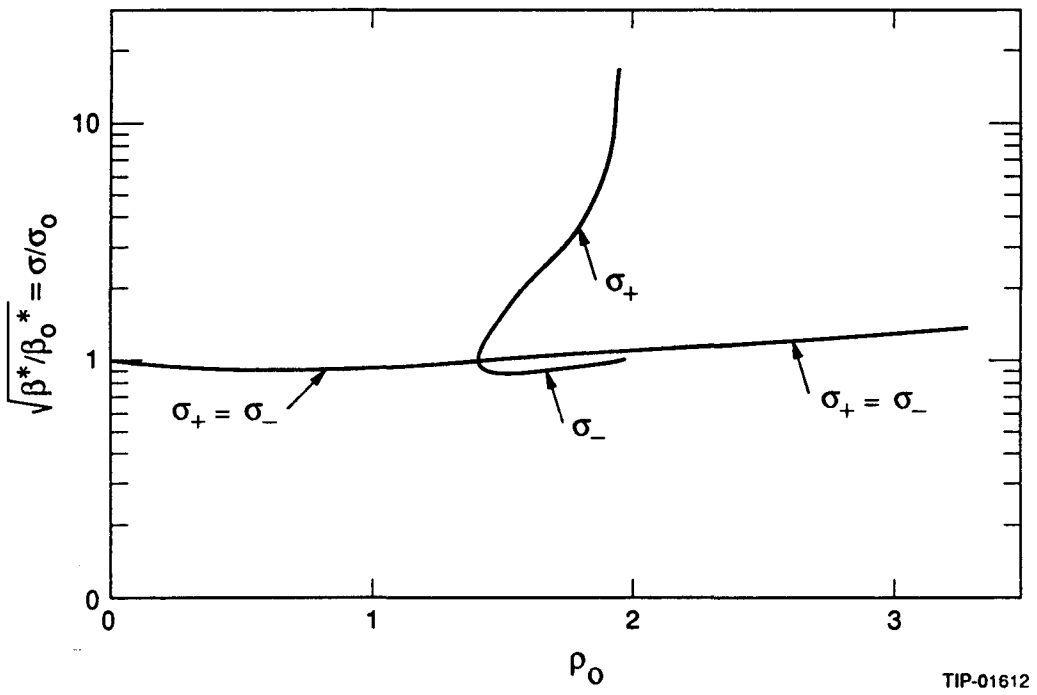

Figure 4. The Dynamic-beta Steady-states.

Note that not all steady-states are stable. In particular, in region (12), it will be shown later that the equal-beam steady-state is in fact unstable; any infinitesimal perturbation will force the beam either to converge into the flip-flop state or to become unstable.

4.0 STEADY-STATE WITH NONLINEAR BEAM-BEAM FORCE

In the previous section, we assumed a linearized beam-beam force. With this assumption, the perturbed steady-state remains gaussian, and only the rms beam size has

changed. However, if the beam distribution is indeed gaussian, the beam-beam force cannot be strictly linear. (Only a uniform elliptical distribution gives strictly linear beam-beam force, and even then, only inside the elliptical region of the distribution.) Therefore an inconsistency exists here. One could consider two ways to proceed:

(a) Include nonlinear beam-beam force for gaussian beams, but insist that the beam-beam force acts only on the second moments of the beam distributions in such a way that the distributions are describable by gaussians. This is still not self-consistent, but hopefully provides useful insights. Additional information on this approach will be provided later.

(b) In general, beam-beam forces and beam distributions are to be found self-consistently. Assuming flat beams for simplicity, the two beam distributions are coupled through the Vlasov equation

$$\begin{aligned} \frac{\partial \Psi_+}{\partial s} + y' \frac{\partial \Psi_+}{\partial y} - F_-(y,s) \frac{\partial \Psi_+}{\partial y'} &= 0 \\ \frac{\partial \Psi_-}{\partial s} + y' \frac{\partial \Psi_-}{\partial y} - F_+(y,s) \frac{\partial \Psi_-}{\partial y'} &= 0 \end{aligned} \tag{13}$$

where

$$\begin{aligned} F_{-,+}(y,s) &= K(s)y + \text{BB force} \\ \text{BB force} &= \frac{2\pi N r_0}{L_x \gamma} \delta_p(s) \textstyle\int_{-\infty}^{+\infty} d\bar{y}\, H(y-\bar{y})\, \rho_{-,+}(\bar{y}) \\ &= \frac{2\pi N r_0}{L_x \gamma} \delta_p(s) \textstyle\int_{-\infty}^{+\infty} d\bar{y}\, H(y-\bar{y}) \textstyle\int_{-\infty}^{+\infty} d\overline{y'}\; \Psi_{-,+}(\bar{y}, \overline{y'}, s)\,. \end{aligned} \tag{14}$$

The external focussing force provided by the accelerator is given by the term $K(s)y$ in Eq. (14). The beam-beam force occurs only at the IP as described by $\delta_p(s)$, the periodic δ-function with period given by the distance between IPs for equally spaced IPs. In a flat beam case, the beam-beam force is obtained by folding the beam distribution $\rho(y)$ with the function $H(x) = 1$ if $x > 0$, and -1 if $x < 0$, as Eq. (14) describes.

The equal-beam, steady-state self-consistent distribution satisfies

$$\partial \Psi_0 / \partial s + y' \partial \Psi_0 / \partial y - F_0(y,s) \partial \Psi_0 / \partial y' = 0 \tag{15}$$

where

$$F_0(y,s) = K(s)y + \text{BB force}$$

$$\text{BB force } = \frac{2\pi N r_0}{L_x \gamma}\, \delta_p(s) \int_{-\infty}^{+\infty} d\bar{y}\, H(y-\bar{y}) \int_{-\infty}^{+\infty} d\overline{y'}\, \Psi_0(\bar{y}, \overline{y'})\,. \tag{16}$$

In the dynamic-beta analysis, it is assumed

$$\text{BB force } \propto \delta_p(s) y\ . \tag{17}$$

With this assumption, the beam-beam problem is soluble, as discussed in the previous section.

It turns out that there exists another soluble case. Consider two relativistic, unbunched, round beams of opposite charges penetrating each other. Let both beams have a distribution that is gaussian in the transverse momental x' and y', and algebraic in coordinates x and y as follows:

$$\Psi_0 = \frac{e\lambda_0 \exp\left[-\dfrac{x'^2+y'^2}{2\sigma'^2}\right]}{2\pi^2 \sigma'^2 A^2 \left(1+\dfrac{x^2+y^2}{A^2}\right)^2} \tag{18}$$

where λ_0 is the line density of the two beams, and $\sigma'^2 = \lambda_0 r_0/\gamma$. It can be shown[7] using the Vlasov equation (15) that if the two beams have the distribution (18) with an arbitrary beam size A, they will pinch each other with their beam-beam forces in such a way that they both maintain the steady-state (18).
Example:

(a) Generalize Eq. (18) by including a uniform, linear external focussing in the derivation.

(b) Find the counterpart of Eq. (18) for the case of flat beams.

In the dynamic-beta model, it was noted that a localized linear beam-beam force (17) drives half-integer resonances $\nu_0 = m/2$. Now note that in the case where the beam-beam force is nonlinear but smooth (nonlocalized, independent of s), as in the case of two self-pinching unbunched beams, a steady-state can be found without indication of resonances, i.e., a nonlocalized nonlinear beam-beam force does not drive resonances.

In general, unfortunately, the beam-beam force is both nonlinear and localized, i.e.,

$$\text{BB force } \propto \delta_p(s) \times (\text{nonlinear function of } y)\,. \tag{19}$$

In this case, like the case in single-particle nonlinear dynamics, the problem becomes very difficult to solve. In particular, resonances are driven when ν_0 is close to a rational number

m/n. A self-consistent strong-strong distribution is yet to be found in this case. The closest soluble problem is that of the weak-strong case when there is only one prominent resonance playing a role.

Drawing analogy with the longitudinal potential-well distortion due to coherent wake fields in a storage ring, it may be stated that in the present case the steady-state solution Ψ_0 is "transverse potential well distorted" by the beam-beam force at the IP.

Assuming the problem is solved, the preceding analysis provides only the equal-beam solution. One could also consider the nonlocal, nonlinear beam-beam forces, and unequal beams, just like we did in the dynamic-beta consideration. This will then give other flip-flop steady-state solutions with nonlinear beam-beam forces. These solutions will be sensitive to the proximity of the tune ν_0 to rational values m/n just like the flip-flop solution in the dynamic-beta model is sensitive to $\nu_0 = m/2$.

5.0 DYNAMICS ABOUT THE STEADY-STATE

Assuming the steady-state, whether the equal-beam or flip-flop solution, is known, the next question to ask is whether the beam motion is stable against small perturbations from it. This is another difficult problem. To approach this problem, consider the steps, arranged in order of complexity, given in Table 1.

Table 1. Steps Taken in Studying the Coherent Beam-beam Dynamics.

Step	Steady-state	Perturbation
1	Unperturbed	center-of-mass motion
2	Unperturbed	rms beam-sizes
3	Dynamic-beta (equal-beam)	rms beam-sizes
4	Unperturbed	higher order modes
5	Dynamic-beta (equal beam)	higher order moments
6	Potential-well distortion (equal beam)	repeat 1–5
7	Flip-flop states	repeat 1–5

Steps 1–4 have been addressed, at least partially, in the literature; some of them are discussed below. Steps 5–7 are yet to be studied.

6.0 RIGID DIPOLE MODEL

As mentioned before, the dynamic-beta effect is the simplest strong-strong model, which involves static beam distortions. The simplest coherent beam-beam model that involves dynamics (moving beams) is the rigid dipole model.[8–15] In this model (step 1 of Table 1), each beam is assumed to have the unperturbed distribution rigidly except that their centers-of-mass are allowed to move in accordance with the beam-beam forces. To illustrate the model, assume the unperturbed beam distribution Ψ_0 is round at the IPs. Let the center-of-mass coordinates of the two beams be designated by $Y_\pm$. For $Y_\pm$ smaller than the beam size so that the beam-beam force can be linearized, the centers-of-mass exert beam-beam kicks on each other according to[16–19]

$$\begin{aligned} \Delta Y'_+ &= -\frac{G}{f}(Y_+ - Y_-) \\ \Delta Y'_- &= -\frac{G}{f}(Y_- - Y_+) \,. \end{aligned} \tag{20}$$

In Eq. (20), f/G is the focal length of the center-of-mass motions, where $f = \beta^*{}_0/4\pi\zeta_0$ is the focal length for incoherent motion and G is a form factor obtained approximately by averaging the single-particle beam-beam kicks over the rigid distribution $\Psi_0(r)$:

$$G = \frac{\int_0^\infty r\,dr\,\Psi_0{}^2(r)}{\Psi_0(0)\int_0^\infty r\,dr\,\Psi_0(r)} = \begin{cases} 1/2 & \text{for round gaussian.} \\ 1 & \text{for round uniform disk.} \end{cases} \tag{21}$$

Equation (21) applies only for round distributions, but it has been shown[18] that $G = 1/2$ even for an elliptical gaussian.

Consider the case of one bunch per beam. The transformation for the vector $[Y_+, Y'_+, Y_-, Y'_-]$ from IP to IP is

$$\begin{bmatrix} 1 & 0 & 0 & 0 \\ -\frac{G}{f} & 1 & \frac{G}{f} & 0 \\ 0 & 0 & 1 & 0 \\ \frac{G}{f} & 0 & -\frac{G}{f} & 1 \end{bmatrix} \times \mathbf{R}\,, \tag{22}$$

where $\mathbf{R}$ is the transformation through the storage ring arcs,

$$\mathbf{R} = \begin{bmatrix} \cos\mu_0 & \beta^*{}_0\sin\mu_0 & 0 & 0 \\ -\frac{1}{\beta^*{}_0}\sin\mu_0 & \cos\mu_0 & 0 & 0 \\ 0 & 0 & \cos\mu_0 & \beta^*{}_0\sin\mu_0 \\ 0 & 0 & -\frac{1}{\beta^*{}_0}\sin\mu_0 & \cos\mu_0 \end{bmatrix} . \tag{23}$$

The transformation matrix (22) can be analyzed for eigenvalues. The four eigenvalues form two complex conjugate pairs: each corresponds to a coherent beam-beam dipole mode: the 0- and the π-mode.

In the 0-mode, the two beams move up and down (or left and right) together, i.e., $Y_+ = Y_-$, at the IP. The coherent beam-beam forces on the centers-of-mass vanish [see Eq. (20)]. The motion is as if unperturbed and is therefore always stable regardless of the beam intensity. The 0-mode coherent frequency μ is equal to the unperturbed frequency μ_0.

In the π-mode, the bunches move out of phase with $Y_+ = -Y_-$ at the IPs. The effective coherent beam separation is therefore $2G$ times that in the incoherent case (G from the form factor, 2 due to both beams moving). The π-mode frequency μ therefore satisfies Eq. (2a) with the replacement $\zeta \to 2G\zeta_0$. This beam-beam system is stable if the π-mode is stable, i.e.,

$$\zeta_0 < \cot(\mu_0/2)/4\pi G\,. \tag{24}$$

In the unstable region, except when ζ is very close to the stability boundary, the instability growth rate obtained from the imaginary part of the eigenvalues of the π-mode is fast, which means it would be difficult to fight this dipole instability by a typical feedback system.[12,20]

According to Eq. (24), resonance occurs when $\mu_0 = \pi$, or $\nu_0 = 1/2$, just like the incoherent and the dynamic-beta cases. Furthermore, for the case of one bunch per beam assumed so far, the stability conditions (4), (5) and (24) all look similar, especially for gaussian beams for which $G = 1/2$. Figure 5, however, illustrates one important difference among them.

Similar analysis can be carried out for M bunches per beam in a storage ring with $2M$ IPs. In this case, the transformation matrix will be $4M \times 4M$ and there are $2M$ coherent dipole modes. Stability of the system requires all modes be stable, i.e., all eigenvalues have $|\lambda| = 1$.

For multiple bunches per beam, the coherent dipole instability distinguishes itself from the incoherent and the dynamic-beta effects in the resonances it excites. In the $M = 1$ case, all three cases excite only the $\nu_0 = m/2$ resonances. For multiple bunches per beam, the difference comes from the fact that the superperiodicity suppresses incoherent effects, but not coherent effects. Let the total tune of the storage ring be $\nu = 2M\nu_0$. (Throughout this paper, the notations μ_0 = phase advance between IPs, ν_0 = tune advance between IPs, and ν = total tune of the storage ring are used.) Coherent dipole instability occurs

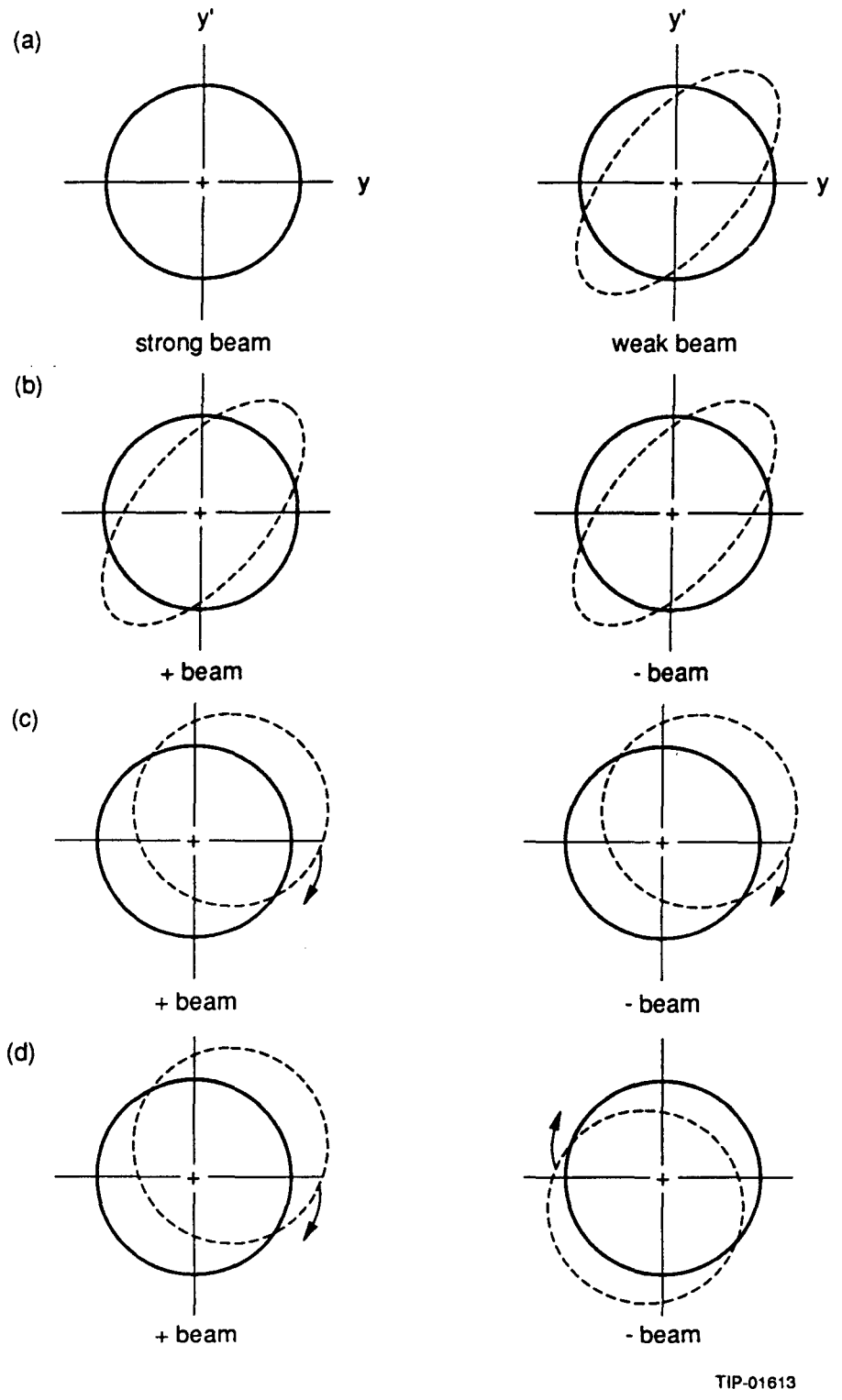

Figure 5. Distributions in Phase Space of Two Colliding Beams for Four Cases: (a) Incoherent Weak-strong Case, (b) Dynamic-beta Effect, (c) Coherent Dipole 0-mode, and (d) Coherent Dipole π-mode. (b), (c) and (d) are Strong-strong Cases. The solid and dashed curves indicate the unperturbed and the beam-beam perturbed distributions, respectively. The perturbed distribution moves with time in (c) and (d) but are static in (a) and (b). The beam dynamics behavior are very distinct in all cases, even though their stability criteria look similar.

when $\nu = m$, while the incoherent and dynamic-beta resonances occur at a much sparser density, i.e., when $\nu = mM$. Coherent effects thus impose stricter limit on beam stability for $M > 1$, and the stability condition no longer look the same as the incoherent and dynamic-beta effects. Figure 6 shows the sawtooth diagrams for the cases of $M = 1, 2, 3$ and 4.

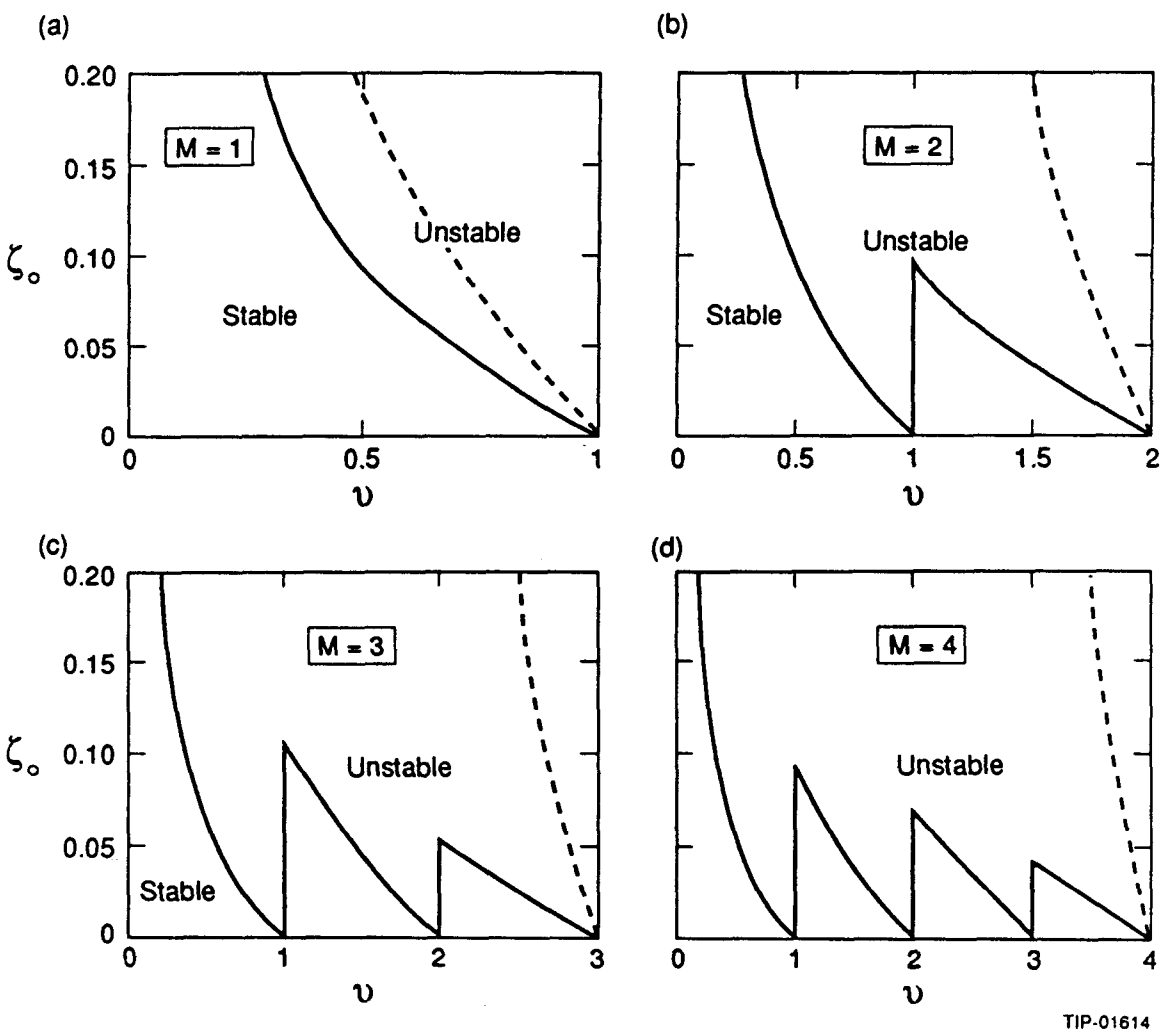

Figure 6. Stability Diagrams (when $G = 1/\sqrt{2}$) for $M = 1, 2, 3, 4$ Bunches per Beam. $\nu = 2M\nu_0$ is the total tune. The figure repeats with a period of $\nu = M$. The dashed curves give the stability region for the weak-strong case for comparison.

Coherent beam-beam dipole modes have been observed in storage rings such as SPEAR,[21] PETRA[22,23] and TRISTAN.[24–26] Figure 7 shows the observation of the 0- and the π-modes in PETRA with $M = 1$.[22] The peak at the lower frequency corresponds

to the 0-mode, the one at higher frequency is the π-mode. In Figure 7(b), the π-mode frequency is slightly shifted because, although separated, the beams still couple slightly. Figure 8 shows the observation in TRISTAN with $M = 2$.[24] The parameters are such that all four modes are stable and these modes are observed by external driving.[18] With proper filtering, selected modes are observed.

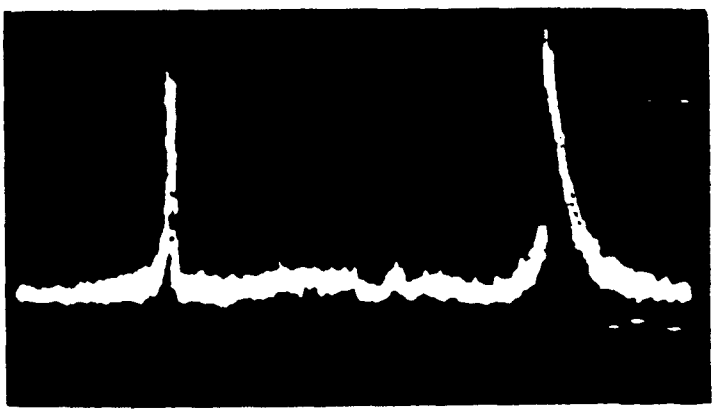

Vertical eigenfrequencies of two colliding bunches.

(a)

Vertical eigenfrequencies of two separated bunches.

(b)

Figure 7. Observation of the 0- and π-modes in PETRA with One Bunch per Beam: (a) Beams Colliding and (b) Separated.

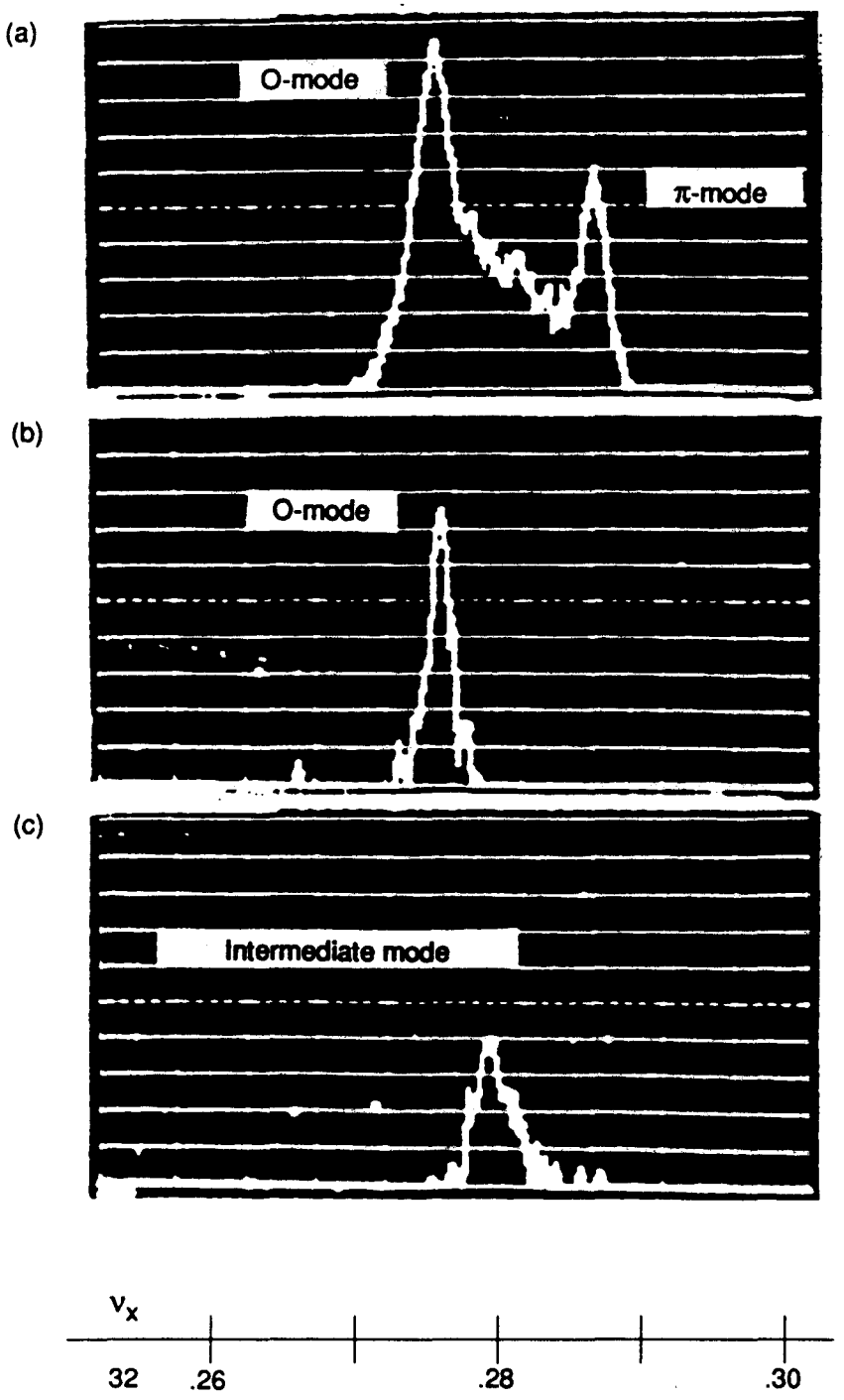

Figure 8. Observation of Coherent Dipole Modes at TRISTAN with 2 Bunches per Beam. (a) Beam spectrum with four modes superimposed. With proper filtering, (b) the 0-mode, and (c) an intermediate mode could be observed.

The dipole instabilities have been studied in the literature more extensively than the other coherent beam-beam effects. Several extensions of the basic model described so far have been worked out.[27] These include:

unequal beams ($N_+ \neq N_-$)[27]

unequal tunes ($\nu_+ \neq \nu_-$)[27]

error in phase advances between IPs[28]

unequal circumferences ($C_+ \neq C_-$)[29,30]

four compensating beams[20]

coherent beam-beam synchro-betatron resonances[31]

spontaneous beam separation[29,32]

long-range beam-beam interactions.[33–37]

One is fact makes the observation that for each incoherent beam-beam effect, there is most likely a coherent counterpart, and vice versa. Some of these extensions are reviewed below.

6.1 Unequal Beams

Consider the case when the two beam bunches have different intensities, $\rho_+ \neq \rho_-$, and the two beams are in separate storage rings with different phase advances between IPs, $\mu_+ \neq \mu_-$. The eigenmode frequencies $\mu_{1,2}$ are determined from[27]

$$2\cos\mu_{1,2} = \cos\mu_+ + \cos\mu_- - G\rho_+ \sin\mu_+ - G\rho_- \sin\mu_- \pm \sqrt{Q} \tag{25}$$

where

$$Q = (\cos\mu_+ - \cos\mu_- - G\rho_+ \sin\mu_+ + G\rho_- \sin\mu_-)^2 + 4G^2\rho_+\rho_- \sin\mu_+ \sin\mu_- \ .$$

Note that this analysis allows other differences in the two beams, e.g. differences in $N_\pm$, $\gamma_\pm$, $\beta^*{}_\pm$ and $\sigma_\pm$ can all be incorporated into $\rho_\pm$.

Example: Show that Eq. (25) reduces to Eq. (2a) when $\mu_+ = \mu_- = \mu_0$ and $\rho_+ = \rho_- = \rho_0$.

Example: When $\rho_+ = 0$, show that the $-$ beam is unperturbed, while the $+$ beam frequency shift $= G \times$ (the incoherent shift). This is the coherent dipole mode in the weak-strong limit.

Example: When $\mu_+ = \mu_- = \mu_0$ but $\rho_+ \neq \rho_-$, show that the two eigenmodes are still described by a 0-mode and a π-mode, and that the mode frequencies are given by

$$\cos\mu = \cos\mu_0 - \begin{bmatrix} 0 \\ 1 \end{bmatrix} G(\rho_+ + \rho_-)\sin\mu_0 \,. \tag{26}$$

6.2 Unequal Tunes

Equation (25) also includes the effect of unequal tunes. Figure 9 shows the stability region in the (ν_{o+}, ν_{o-}) plane.[27] A new set of sum resonances $\nu_{o+} + \nu_{o-} = m$ is introduced, where $\nu_{o\pm} = \mu_{o\pm}/2\pi$ are the tune advances between IPs in the two storage rings. Strictly speaking, only these sum resonances are true coupled-beam modes. Coherent beam-beam modes are strongly excited by the sum resonances.

In passing, it can be noted that splitting ν_{o+} and ν_{o-} did not improve the instability. The possible expectation that splitting the tunes introduces Landau damping, and therefore stability, to the system is incorrect.

6.3 Phase Advance Errors

Consider again the case with one bunch-per-beam. In the previous analysis, the two IPs in the storage ring are separated by two arcs with equal betatron phase advances. The analysis can be extended to unequal phase advances parametrized as $\mu_0 \pm \delta\mu$.[9] The result is shown in Figure 10(a). The most pronounced new feature is the introduction of a stopband when the total tune $\nu = 2\nu_0$ is close to 1/2. The stopband edges are found to be

$$\zeta_0 = \frac{\cot\mu_0}{2G\pi}\,\frac{1 \pm \sin\delta\mu}{\cos^2\delta\mu} \,. \tag{27}$$

The sawtooth part of the stability boundary becomes [Cf. Eq. (24)]

$$\zeta_0 = \frac{\sin\mu_0}{4G\pi(\cos\delta\mu - \cos\mu_0)} \,. \tag{28}$$

Equation (28) reduces to (24) if $\delta\mu = 0$. For multiple bunches per beam, the results resemble Figure 6, except that new stopbands of complicated structure are created around half-integer resonances $\nu = m/2$. Figure 10(b) shows the result obtained numerically for the case of $M = 2$.[28]

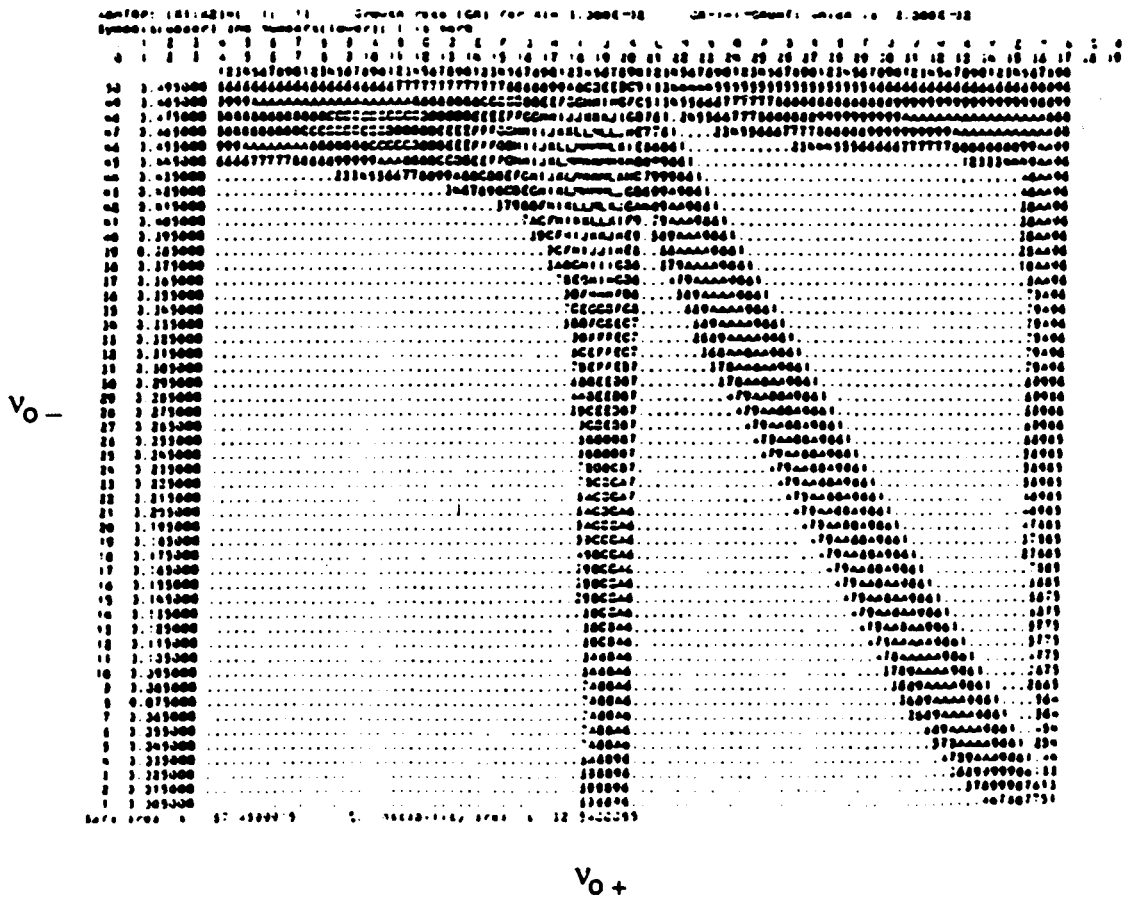

Figure 9. Stability Diagram in (ν_{o+}, ν_{o-}) Space, which Shows the Excitation of Sum Resonances $\nu_{o+} + \nu_{o-} = m$. The horizontal ν_{o+} axis is from 0 to 1. The vertical ν_{o-} axis is from 0 to 1/2. The pattern repeats if $\nu_{o\pm}$ are replaced by $\nu_{o\pm} + 1/2$.

6.4 Unequal Circumferences

Consider the case when the two beams are stored in separate storage rings of different circumferences $C_\pm$. The number of bunches $K_\pm$ are chosen so as to have a fixed bunch spacing $C_+/K_+ = C_-/K_-$. The system has a superperiod $= K_+C_- = K_-C_+$. The total tune advances per superperiod of the two storage rings are $K_+\nu_{o-}$ and $K_-\nu_{o+}$. The coherent dipole beam-beam resonances in this system are given by

$$K_+\nu_{o-} = m/2 \tag{29a}$$

$$K_-\nu_{o+} = m/2 \tag{29b}$$

$$K_+\nu_{o-} + K_-\nu_{o+} = m\,. \tag{29c}$$

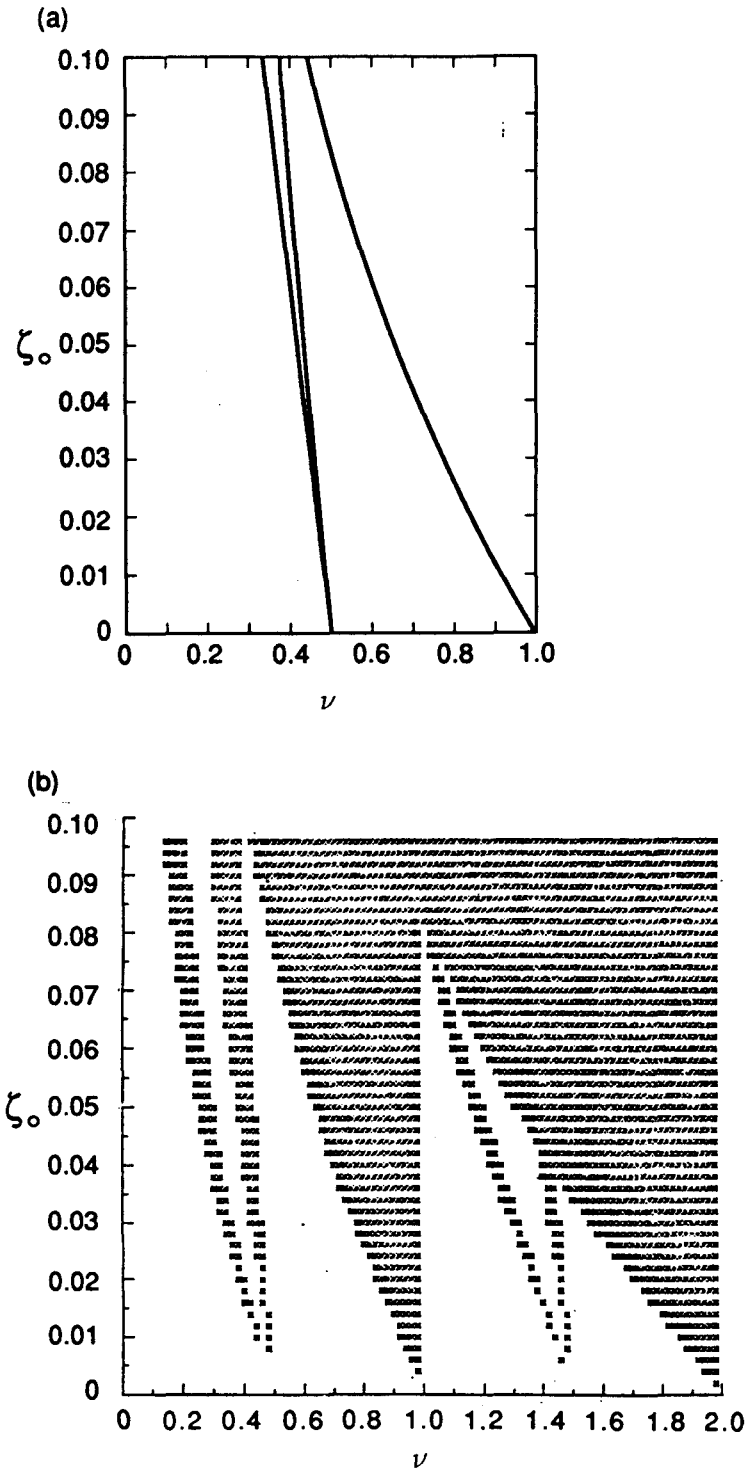

Figure 10. Effect of Phase Advance Errors in the Storage Ring Arcs on the Sawtooth Diagram. (a) $M = 1$, $\delta\mu/2\pi = 0.02$. (b) $M = 2$, $\delta\mu/2\pi = 0.03$. The form factor is taken to be $G = 1$.

The consequence is that there are now many more resonances, which makes it undesirable to have unequal circumferences for the two beams.[30]

Figure 11 shows the result for the case $K_+ = 2$, $K_- = 3$.[29,30] Note particularly the three coupling resonances of the type (29c), which are strongly driven by the beam-beam coupling. In comparison, the single-beam resonances of types (29a) and (29b) are driven only when $\nu_{o\pm} = m/2$.

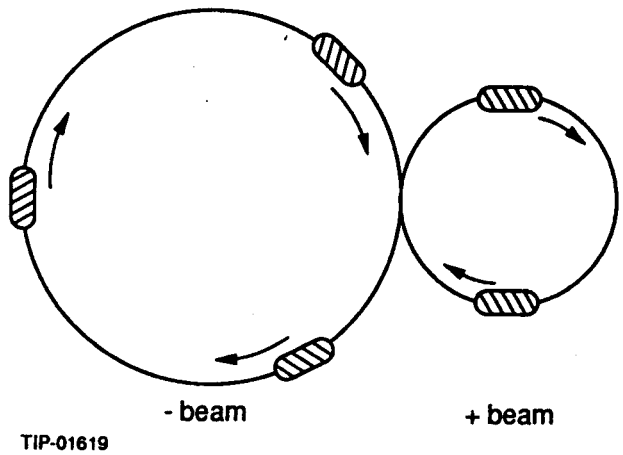

Figure 11. (a) Unequal Circumferences for the Case $K_+ = 2$, $K_- = 3$.

6.5 Four Beam Compensation

One method to compensate for the beam-beam effect—therefore greatly increasing the luminosity—is the four-beam idea of DCI.[38,39] In this idea, two beam bunches +Ne and −Ne are made to collide with two other beam bunches +Ne and −Ne, as shown in Figure 12(a). The colliding bunches have neutral net charges and thus presumably produce no beam-beam forces. Unfortunately, this idea had not worked at DCI.

The problem is that what has been eliminated is the incoherent beam-beam force. Coherent beam-beam forces are not dealt with, because infinitesimal deviations from the steady-state can still grow as coherent modes. In fact, this four-beam combination has worsened the coherent beam-beam effect. The net result is that one problem has been traded for another—better incoherent effects for worse coherent effects.

Figure 12(b) illustrates the sawtooth diagram for the four-beam case.[20] The stability boundary consists of two segments, separated at $\nu = 1/2$. The segment below $\nu = 1/2$ turns out to be close to what would be obtained with colliding −Ne and −Ne (or +Ne and

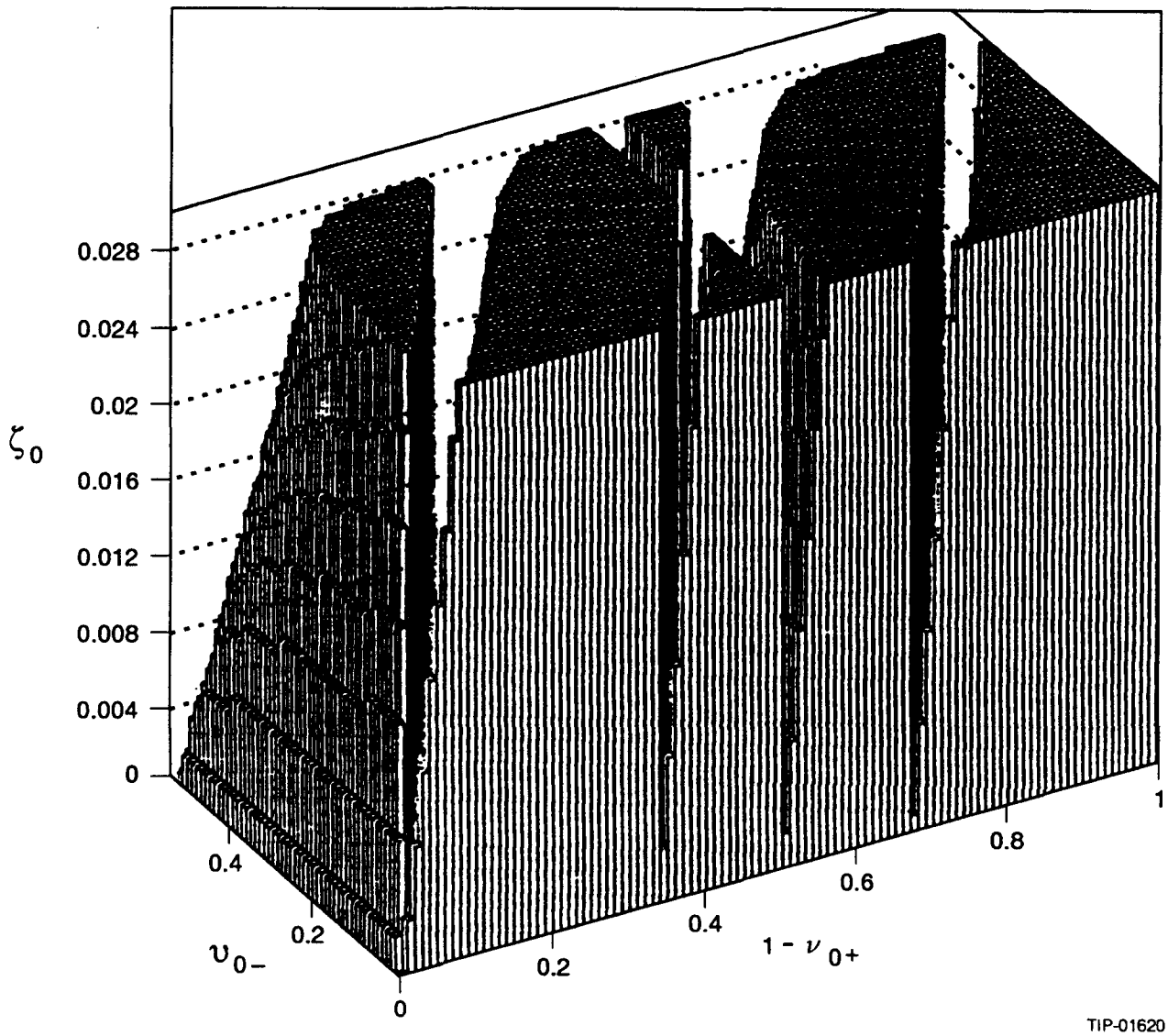

Figure 11. (b) Maximum Stable ζ_0 Value Plotted in the (ν_{o+}, ν_{o-}) Plane, Showing Three Coupling Resonances of Type (29c).

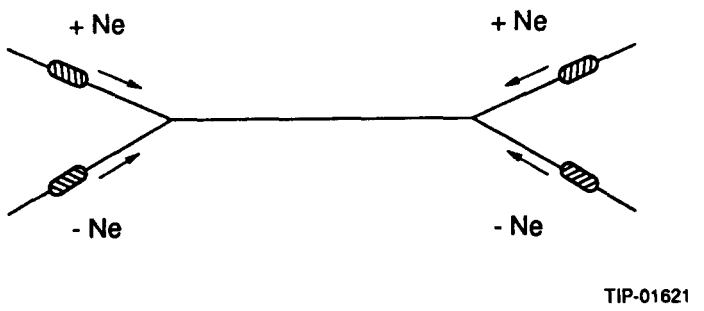

(a)

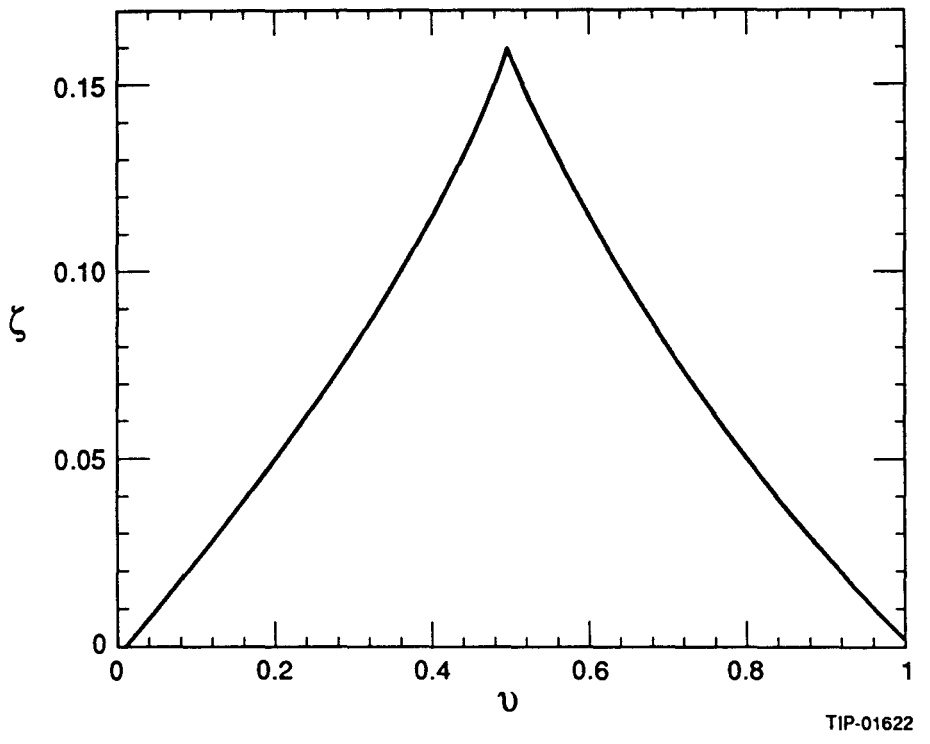

(b)

Figure 12. (a) Schematic of the Four-beam Compensation Arrangement.
(b) Stability Diagram for the 4-beam Scheme.

+Ne), while the segment above $\nu = 1/2$ is close to that for colliding +Ne and −Ne. The coherent dipole instability therefore is a result of the worst of the two possible combinations.

The situation would change if the four colliding beams are provided by linac colliders instead of storage rings, in which case the beams are discarded after collision. There will be no coherent beam-beam effects (at least not the multi-turn resonant type of interest here), and the four-beam idea could still be applied to avoid beamstrahlung, which is one of the main limiting effects of high energy linac colliders. In fact, only three beams are needed to come from linac colliders; one beam can still come from a storage ring.

Also, analyses have been carried out for the four-beam scheme for higher order modes using Vlasov techniques.[40–45] One such analysis[41] yields the result shown in Figure 13. Additional information on the Vlasov technique for higher order modes is provided later.

6.6 Synchro-betatron Resonances

Finite dispersions at the IP or the rf cavity excite coherent beam-beam synchro-betatron difference resonances $\nu_\beta - n\nu_s = m$. Similar to the single-particle case, the sum resonances are stable above transition.

The analysis has been done when the beam-beam force is linearized,[31] in which case only the linear resonances ($n = 1$) are excited. The dynamics can be described by 8×8 transformation matrices. Eigen-analysis of the system gives the stability region in the (ν_β, ν_s) space as shown in Figure 14, where ν_β and ν_s are the total betatron and synchrotron tunes. The synchro-betatron resonances occupy small regions in the tune diagram even with exaggerated values of dispersion at the IP and the rf cavity as used in Figure 14, and are therefore not a very significant concern in practice.

6.7 Spontaneous Beam Separation

So far in analyzing the coherent dipole effects, we have linearized the beam-beam force. This is valid only for center-of-mass motions small compared with the beam size σ. It suffices if one is interested only in the beam-beam effect on luminosity because even small beam motion must be avoided for luminosity purposes. The rigid dipole motion in the presence of nonlinear beam-beam forces has been simulated numerically. Figure 15 shows one such result.[14]

With a nonlinear beam-beam force, the magnitude of center-of-mass motion saturates when beam separation becomes comparable to σ. In fact, as beams separate far enough, they can find a steady-state separation to stay in. For example, in case of 1 bunch per beam with round, gaussian, equal beams, the steady-state beam separation is zero in the linearly stable region $2\pi\zeta_0 < \cot(\mu_0/2)$, while in the unstable region, the steady-state beam

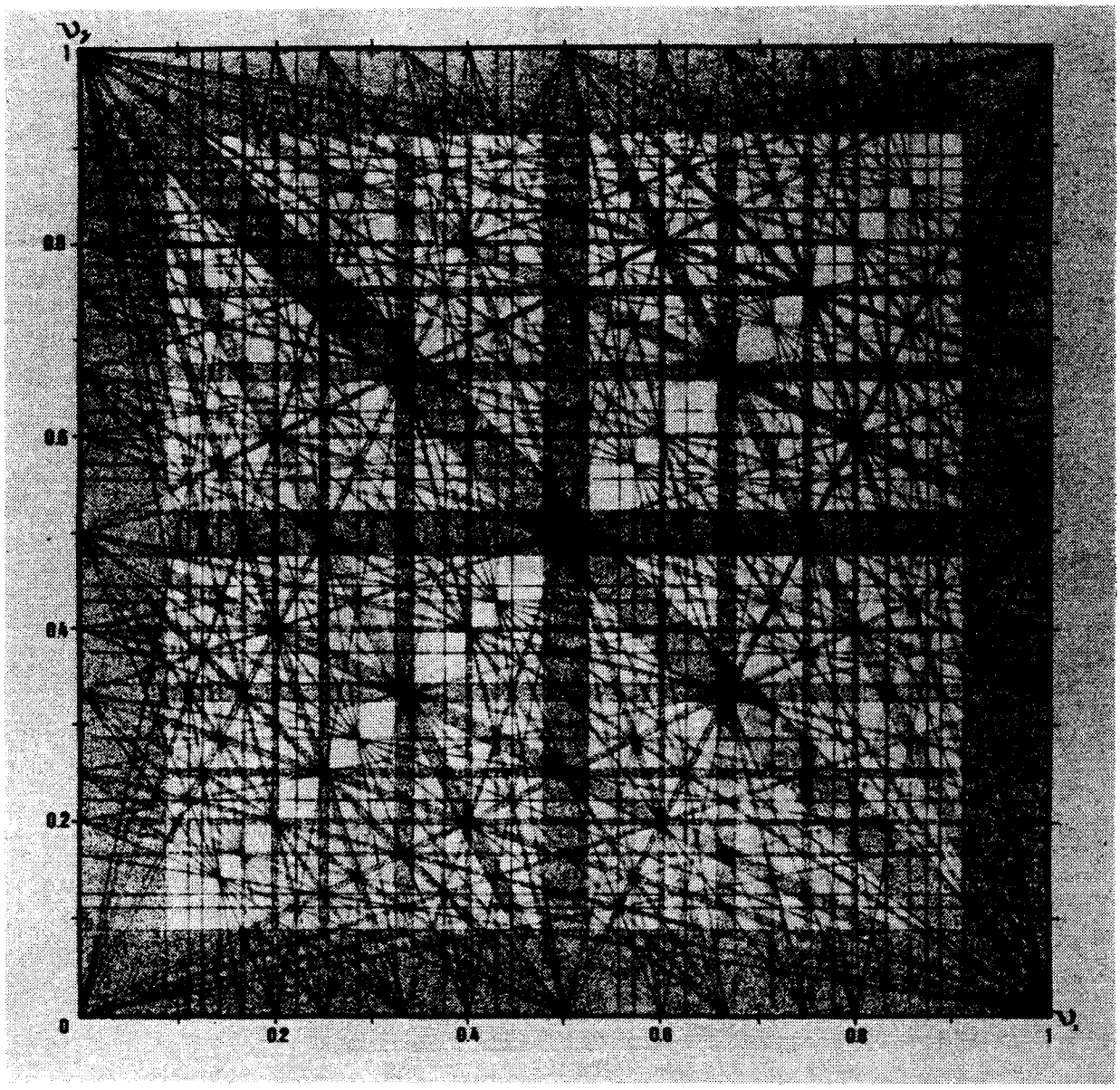

Figure 13. Stability Region in (ν_x, ν_y) Space for DCI with $\zeta_0 = 0.05$, According to a Mode Analysis.

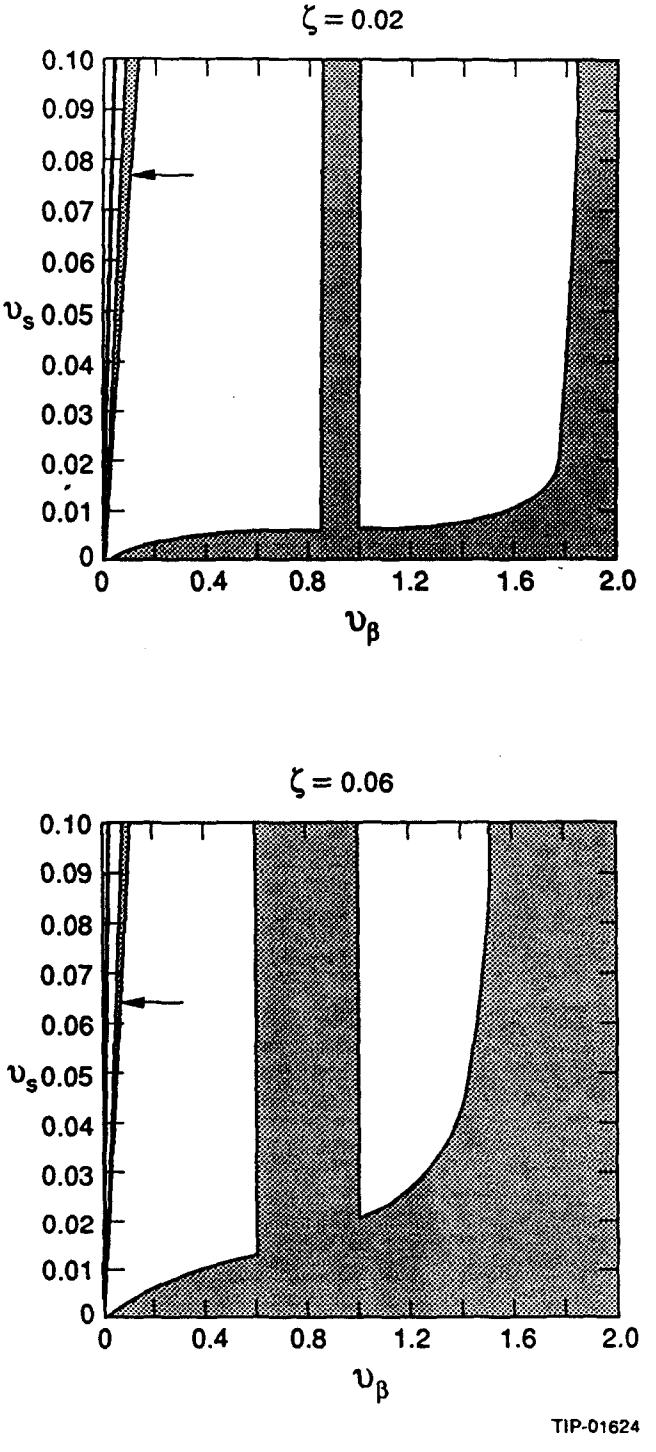

Figure 14. Stability Region in the (ν_β, ν_s) Space for Two Values of $\zeta_0 = 0.02$ and 0.06. The instability regions due to synchro-betatron resonances as indicated by arrows.

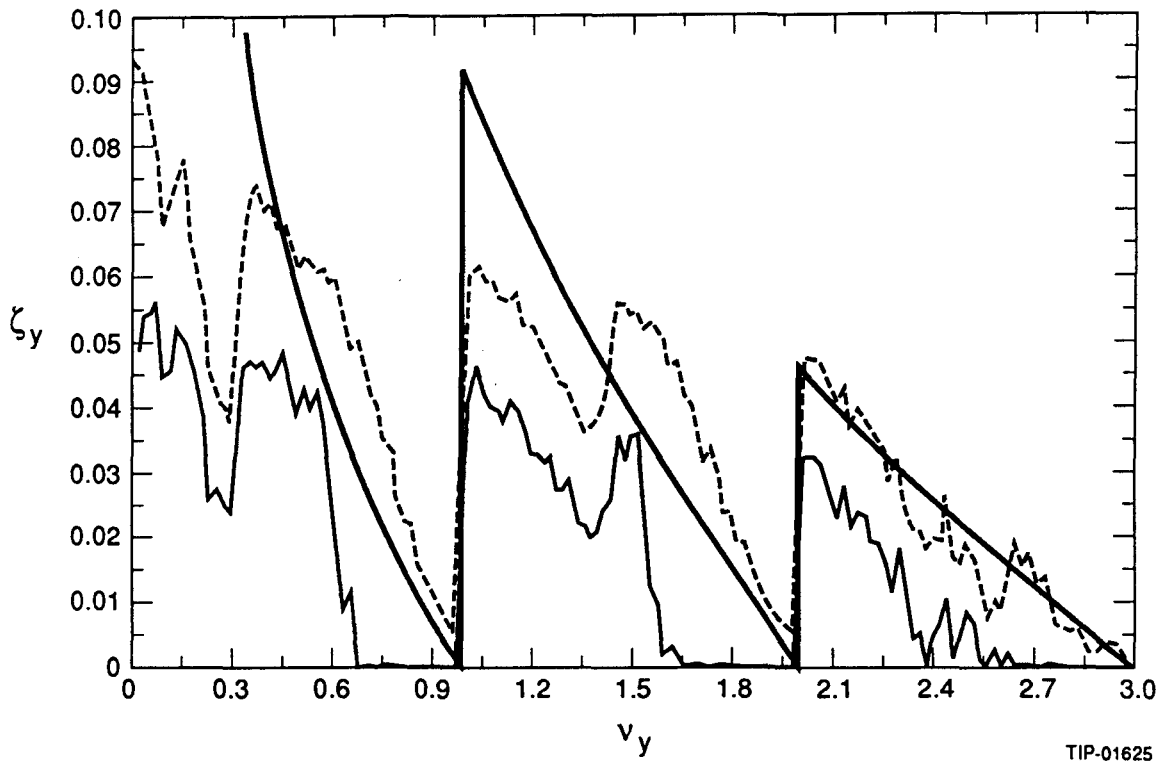

Figure 15. The Value of ζ_y as a Function of the Total Vertical Tune ν_y and Fixed $\nu_x = 0.2$ for the Case of $M = 3$. Rigid center-of-mass motions are simulated with nonlinear beam-beam forces. Solid and dotted curves represent the minimum and average values of ζ_y over 200 turns simulated. Sawtooth curve is that predicted by a linear theory.

separation Δ is determined by

$$\frac{2\sigma^2}{\Delta^2}(1 - e^{-\Delta^2/2\sigma^2}) = \frac{\cot\frac{\mu_0}{2}}{2\pi\zeta_0} < 1\,. \tag{30}$$

With beams separated, the luminosity is reduced by a factor $\exp(-\Delta^2/4\sigma^2)$. Figure 16 shows the behavior of Δ/σ and luminosity reduction factor as functions of the stability parameter $x = 2\pi\zeta_0/\cot(\mu_0/2)$.

It may be desirable to study the behavior of small perturbations around a separated-beam configuration. The analysis will yield the corresponding mode frequencies and the stability conditions. The case of unequal tunes has also been studied. It was found that the behavior of beam separation becomes complicated near a sum resonance $\nu_{o-} + \nu_{o+} = m$.[29,32]

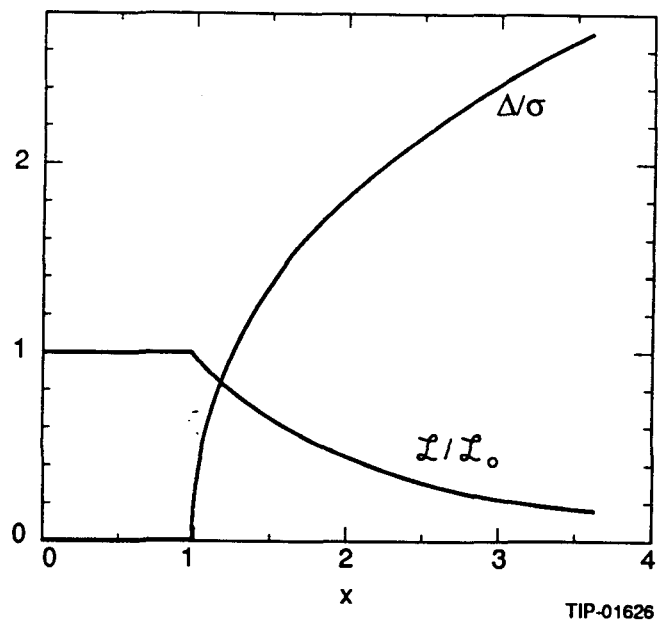

Figure 16. Steady-state Beam Separation due to Nonlinear Beam-beam Forces. (a) Δ/σ as a function of $x = 2\pi\zeta_0/\cot(\mu_0/2)$. (b) Luminosity reduction as function of x.

7.0 QUADRUPOLE MODES

In the dipole model, the beam distribution is assumed to be rigid; only center-of-mass motions are allowed. In general, coherent beam motion is to be described as a superposition of all modes, not only dipole modes. The dynamics of these modes altogether will determine the stability of the beam. When proceeding to higher order modes, more resonances will play a role, as shown in Table 2.

Table 2. Coherent Beam-beam Modes and Their Driving Resonances.

Mode	Driving Resonances
rigid dipole	total tune $\nu = m$
quadrupole	$\nu = m/2$
sextupole	$\nu = m/3$
etc.	

Consider two bunches colliding head-on (i.e., no dipole motion), but their beam sizes oscillate (i.e., they execute quadrupole oscillation). Define the Σ-matrix by the second

moments as

$$\Sigma = \begin{bmatrix} \langle x^2 \rangle & \langle xx' \rangle & 0 & 0 \\ \langle xx' \rangle & \langle x'^2 \rangle & 0 & 0 \\ 0 & 0 & \langle y^2 \rangle & \langle yy' \rangle \\ 0 & 0 & \langle yy' \rangle & \langle y'^2 \rangle \end{bmatrix} . \tag{31}$$

There is a Σ-matrix for each beam. Designate the two Σ-matrices by $\Sigma_\pm$. The transformations through the arcs are:

$$(\Sigma_\pm)_{\text{out}} = \mathbf{R}\,(\Sigma_\pm)_{\text{in}}\,\widetilde{\mathbf{R}} \tag{32}$$

where the matrix $\mathbf{R}$ is the same as that defined in Eq. (23), if $\beta^*{}_{x0} = \beta^*{}_{y0} = \beta^*{}_0$ and $\mu_{x0} = \mu_{y0} = \mu_0$.

As indicated by Table 2, nonlinear dynamics plays a fundamental role in the coherent beam-beam dynamics. Unlike the single-particle nonlinear dynamics, however, even a linearlized beam-beam force is capable of driving nonlinear resonances because the focal lengths depend on the beam sizes. The transformation of the Σ-matrices through the IP due to a linearized beam-beam force is given by

$$\begin{aligned} (\Sigma_+)_{\text{out}} &= \mathbf{T}_{\text{BB}-}(\Sigma_+)_{\text{in}}\,\widetilde{\mathbf{T}_{\text{BB}-}} \\ (\Sigma_-)_{\text{out}} &= \mathbf{T}_{\text{BB}+}(\Sigma_-)_{\text{in}}\,\widetilde{\mathbf{T}_{\text{BB}+}} \,. \end{aligned} \tag{33}$$

$\mathbf{T}_{\text{BB}\pm}$ are the beam-beam matrices

$$\mathbf{T}_{\text{BB}\pm} = \begin{bmatrix} 1 & 0 & 0 & 0 \\ -\frac{1}{f_{x\pm}} & 1 & 0 & 0 \\ 0 & 0 & 1 & 0 \\ 0 & 0 & -\frac{1}{f_{y\pm}} & 1 \end{bmatrix} \tag{34}$$

which gives the effect on the beam size of one beam at IP due to the oscillating size of the other beam. The focal lengths $f_{x\pm}$ and $f_{y\pm}$ depend on $\sigma_{x\pm} = \langle x^2 \rangle^{1/2}$ and $\sigma_{y\pm} = \langle y^2 \rangle^{1/2}$ which are the instantaneous, oscillating beam sizes of the two beams.

Consider small perturbations around a steady-state Σ_0:

$$\Sigma_- = \Sigma_0 + \Delta\Sigma_-, \qquad \Sigma_+ = \Sigma_0 + \Delta\Sigma_+. \tag{35}$$

To simplify the analysis, assume the unperturbed beams are round. Next linearize the system of equations (32) – (34) with respect to the infinitesimal elements in the matrices

$\Delta\Sigma_\pm$. Since each beam has six elements $\Delta\langle x^2\rangle$, $\Delta\langle xx'\rangle$, $\Delta\langle x'^2\rangle$, $\Delta\langle y^2\rangle$, $\Delta\langle yy'\rangle$, and $\Delta\langle y'^2\rangle$, the dynamics of the system can be described by 12×12 transformation matrices. Eigen-analysis of the system then gives 6 modes. The result[46] is that four of the twelve eigenvalues are identically unity. They correspond to the two constants of the motion $\langle x^2\rangle\langle x'^2\rangle - \langle xx'\rangle^2$ and $\langle y^2\rangle\langle y'^2\rangle - \langle yy'\rangle^2$. The remaining four dynamic modes have frequencies[47]

$$\cos\mu = \cos 2\bar{\mu} + \begin{bmatrix} 2 \\ 1 \\ -1 \\ -2 \end{bmatrix} \rho_0 \sin\mu_0 \cos\bar{\mu}$$

$$\cos\bar{\mu} = \cos\mu_0 - \rho_0 \sin\mu_0 \,. \tag{36}$$

This result resembles Eq. (2a), although the dynamics is very different. The sawtooth diagram of the system is shown in Figure 17(a). Quadrupole instabilities are most pronounced near resonances $\nu = m/2$.

Similar analysis has been carried out for multiple bunches per beam, in which case there are $4M$ dynamic modes. Figure 17(b) gives the sawtooth diagram for the case of $M = 3$. Again, resonances occur when the total tune is half-integral.

Just like the dipole case, it is possible to extend the basic model described above for the quadrupole modes.[47] For example, one could include in the analysis the phase advance errors to obtain Figure 18. One observes that the phase errors introduce new resonances at $\nu = m/4$. Similar procedure can be extended to the case $\nu_x \neq \nu_y$ to yield Figure 19, which shows structures near the coupling sum resonances $\nu_x + \nu_y = m$.

8.0 QUADRUPOLE MODES AROUND DYNAMIC-BETA

The previous section addresses the quadrupole oscillations around the unperturbed state. One may also investigate quadrupole oscillations around the dynamic-beta steady-state, i.e., that shown in Figure 4. This will give information on whether the beams will choose to stay in the equal-beam, the flip-flop, or neither state. There have been two investigations in this direction using two models, as discussed next.[48]

8.1 The First Model

In this model,[49–51] the dynamics of the second moments is still given by Eqs. (32) – (34) and the beam-beam force is still linearized, but this time the infinitesimal quantities $\Delta\Sigma_\pm$ are not introduced and the problem is not linearized with respect to them. The problem is then studied by numerical simulation. Figure 20(a)[49] shows the equal-beam and the

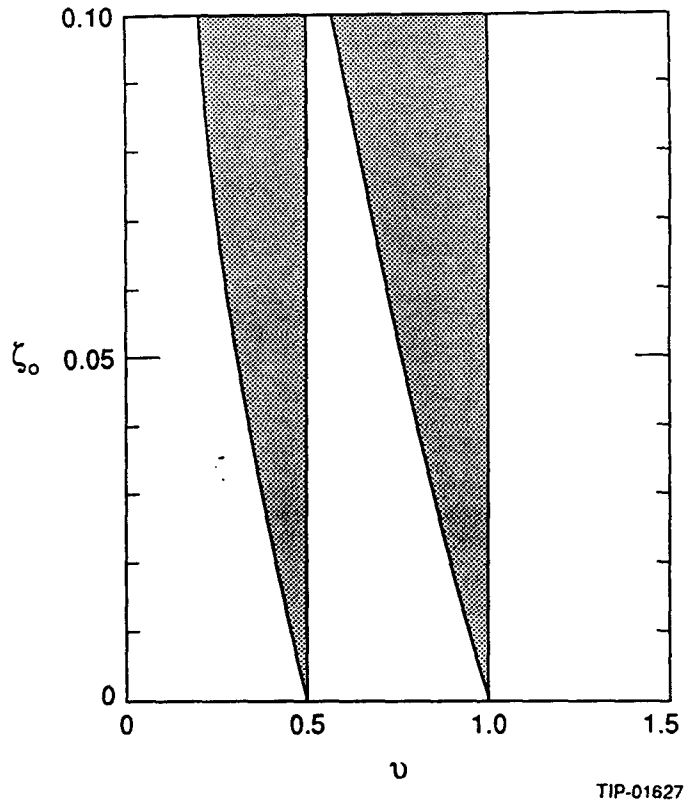

(a)

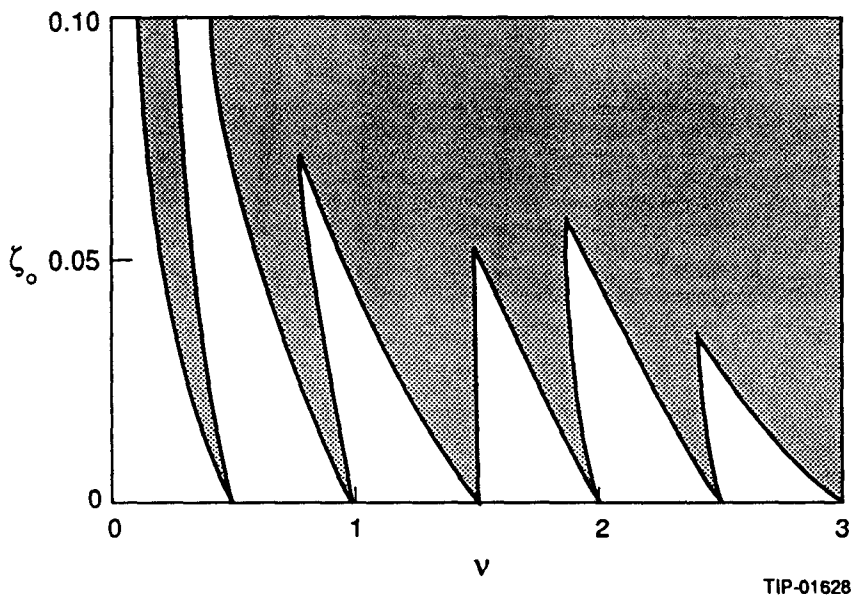

(b)

Figure 17. Sawtooth Diagrams for Coherent Quadrupole Modes. Unperturbed beams are assumed to be round. (a) $M = 1$. (b) $M = 3$. Resonances occur around $\nu = m/2$.

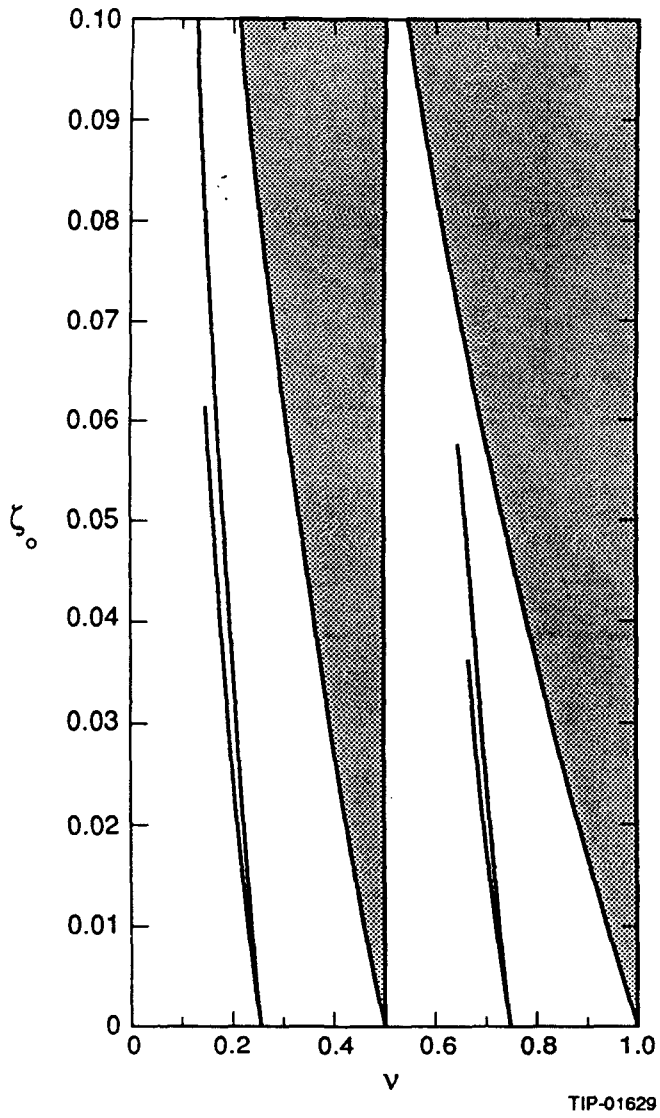

Figure 18. Quadrupole Mode Sawtooth Diagram when Phase Advance Errors $\pm 2\pi \times 0.05$ are Introduced in the Storage Ring Arcs. Stopbands are created near $\nu = m/4$.

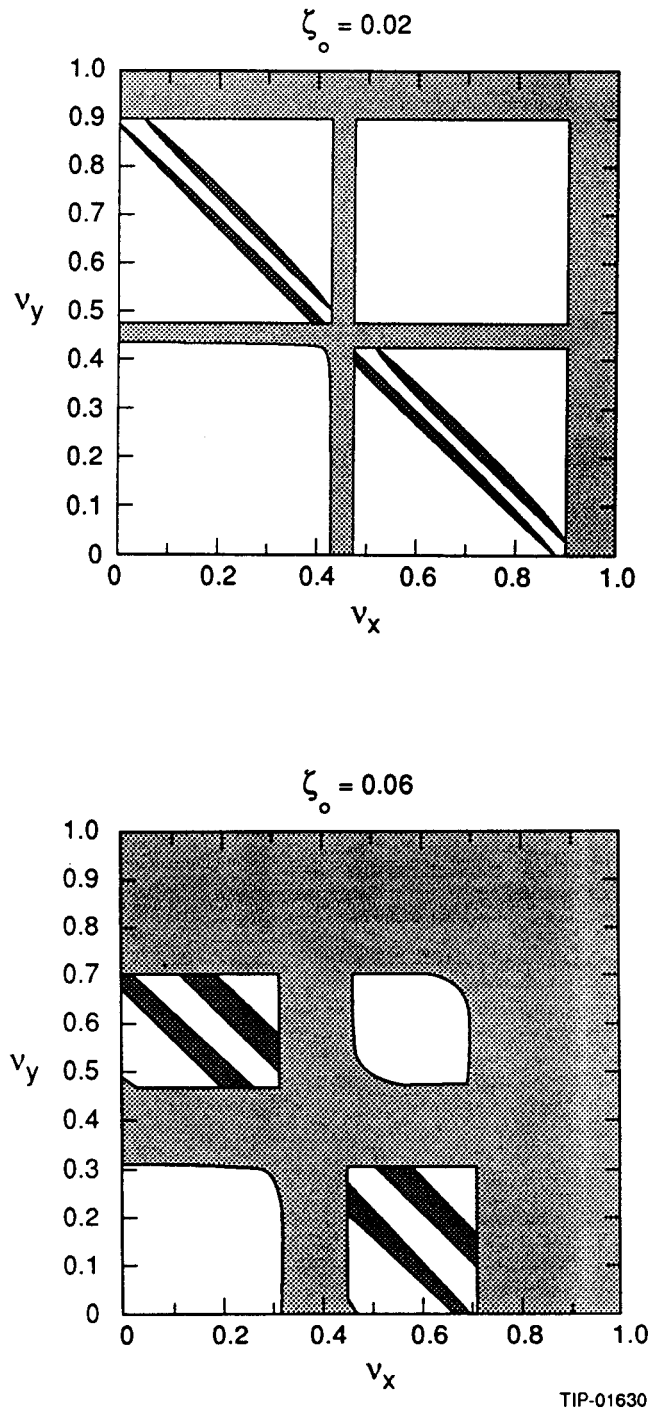

Figure 19. Quadrupole Mode Stability Region in the (ν_x, ν_y) Space for the Case $M = 1$ and Round Beams, for Two Values of $\zeta_0 = 0.02$ and 0.06. Resonances occur when $\nu_x = m/2$, $\nu_y = m/2$, and $\nu_x + \nu_y = m$. No phase errors in arcs are included.

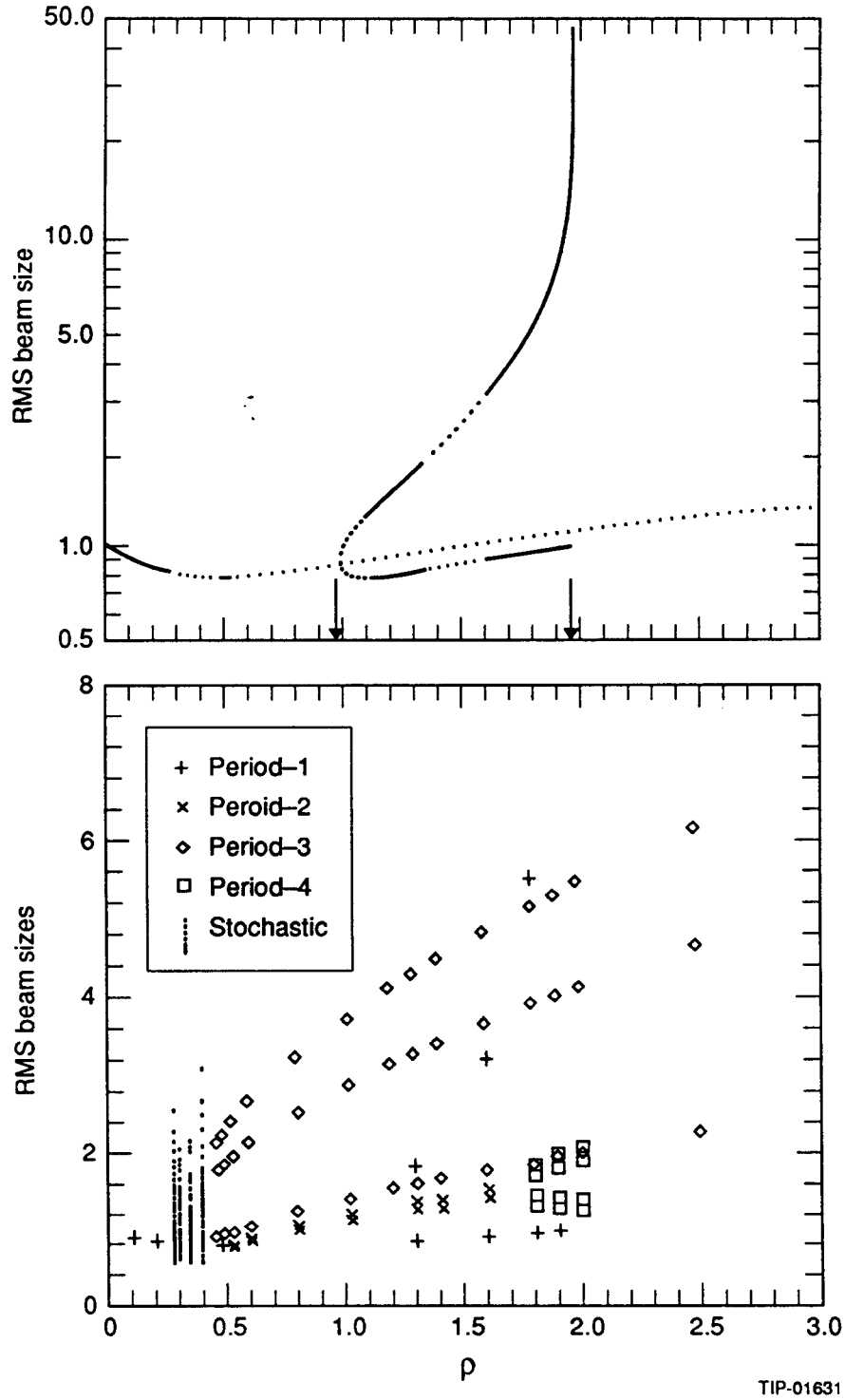

Figure 20. Stability of the Dynamic-beta Steady-state Solutions for the Case of Linearized Beam-beam Force. (a) Period-1 fixed points. Regions stable and unstable against small perturbations are plotted as solid and dotted curves respectively. (b) More complicated motions of second moments are indicated by higher order periods and chaos.

flip-flop solutions, like Figure 4 but slightly different (e.g. a small radiation damping has been included). Solid and dotted sections in Figure 20(a) indicate stable and unstable regions of the steady-states. Note that the equal-beam steady-state is unstable when the flip-flop state exists. In the region ρ less than approximately 0.25, the equal-beam solution is stable. In the present model, $\rho = 0.25$, which corresponds to a beam-beam strength of $\zeta = \rho/2\pi = 0.04$, may be associated with the beam-beam limit observed in colliding beam storage rings. Beyond this region, the equal-beam solution is unstable except for a very small region around $\rho = 0.5$. Between approximately $\rho = 1$ and $\rho = 2$, there are regions where the flip-flop state is stable, meaning the beams will choose to have one beam statically blown-up and the other beam pinched. In the rest of the regions, both the equal-beam and flip-flop steady-states are unstable.

Figure 20(b) shows more details of what is happening to the beams. First, the steady-states are found when they are stable; these agree with Figure 20(a) and are indicated as period-1 states in Figure 20(b). In addition, states with higher periods are found. In a period-2 state, for example, the beams have two states (two sizes) to stay in, and they occupy these two states alternately from one IP to the next. Similarly there are period-3 and -4 states as indicated. In the region approximately between $\rho = 0.25$ to 0.4, the motion of the second moments is apparently chaotic. Figure 20(b) thus shows a rather complex dynamics of the quadrupole modes.

8.2 The Second Model

As mentioned before, linear beam-beam force is inconsistent with gaussian distribution. Insisting on linear beam-beam force in the previous model has violated the Maxwell equations.

Below we introduce another simplified quadrupole mode model[52–54] in which (a) beam distributions are gaussian, (b) the beam-beam force is that for gaussian distributions, therefore nonlinear, but (c) the beam-beam force affects only the second moments in such a way that the beam distribution remains always gaussian. Effects of the nonlinear beam-beam force on higher moments are ignored. Obviously this model is still not self-consistent because of step (c). Although step (b) has rescued the Maxwell equations, step (c) makes the system nonsymplectic, thus violating the Hamiltonian feature which might be important when studying stability of the dynamical system.

One then proceeds as before, i.e., to obtain the dynamic-beta and the flip-flop solutions, and the quadrupole mode dynamics around them. This model has been extensively studied. One interesting result of the study is Figure 21 which shows the steady-state solutions and their stability.[54] Note that although the qualitative behavior of the equal-beam and flip-

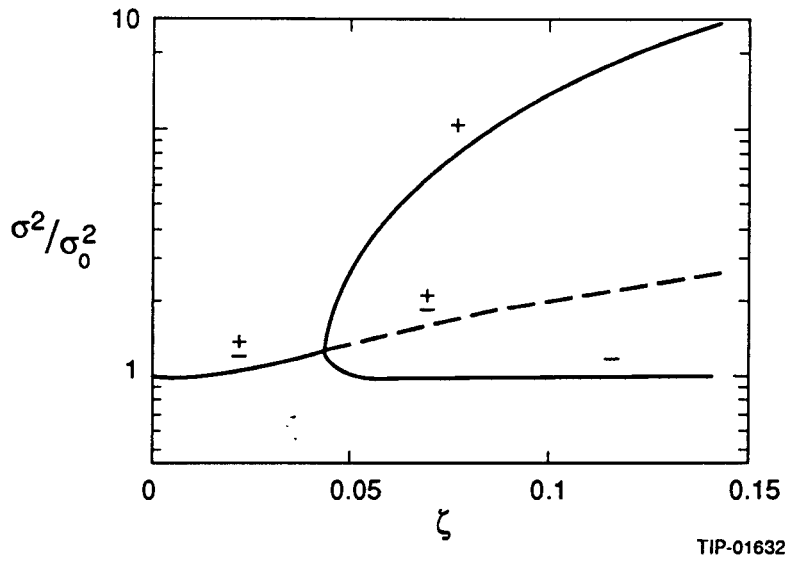

Figure 21. Dynamic-beta Steady-states and Their Stability for a Nonlinear Beam-beam Model. No complicated behavior as Figure 20(b) is observed in this model.

flop states looks similar to that of Figure 20(a), their stability behavior is quite different. In Figure 21, there is always a stable steady-state for the beams to stay in. Below $\zeta \approx 0.05$, the beams stay in the equal-beam state, while they stay in the flip-flop state above $\zeta \approx 0.05$. The behavior is much simpler than that of Figure 20(b). Table 3 is a comparison between the two models.

Table 3. Comparison Between the Two Simplified Quadrupole Mode Models.

	First Model	Second Model
Self-consistency		
Maxwell equations	no	yes
Nonlinear dynamics	yes	no
Dynamic-beta	yes	yes
Flip-flop	yes	yes
Chaos	yes	no
First instability encountered	chaos	flip-flop

It is not very useful to ask which of the two models is more correct because neither is, each having violated something fundamental. However, they do provide information on what to expect in the ultimate analysis.

9.0 HIGHER ORDER MOMENTS

To improve beyond the two models discussed in the previous section, it becomes necessary to deal with nonlinear beam-beam force, and allow this beam-beam force to distort the distribution from gaussian. It is clear that a self-consistent treatment that takes into account all moments is needed here.[40–45,55–62] In other words, we have to consider, in addition to the dipole and quadrupole modes, also the sextupole and octupole modes, etc. A proper treatment will simultaneously be symplectic, and satisfy the Maxwell equations, at least in principle, at the cost of a more complicated analysis.

Use the octupole mode as an example. It can be unstable due to the beam-beam interaction according to the mechanism shown in Figure 22. Let Figure 22(a) be the unperturbed beam distribution in the phase space (y, y') for the two beams. To investigate the coherent octupole mode stability, perturb one of the beams slightly in an octupolar manner as shown in Figure 22(b). This perturbation will couple to the other beam through the beam-beam interaction. For example, the octupolar modulations of the two beams may interlace each other at the IPs as one possible mode pattern. If the motion is stable, the coupled octupolar motion will remain small, as shown in Figure 22(c). However, if the total betatron tune is sufficiently close to a quarter-integer, i.e., $\nu \approx m/4$, the small perturbations will grow exponentially as shown in Figure 22(d), resulting in an octupole mode instability.

In general, instability occurs near resonances $\nu \approx m/n$, as in the incoherent case. However, analogous to the situation shown in Figure 5, there is one important difference in phase space. The cases of incoherent effect, the dynamic-beta effect and the octupole mode effect when $\nu \approx m/4$ (tune per superperiod $\approx m/8$) are illustrated in Figure 23 for one bunch per beam. Note that the dynamic-beta state mentioned in Figure 23 is not that of Figure 4 with linearized beam-beam force, but that mentioned in the discussion following Eq. (19).

The Vlasov equation (13–14) provides a tool for the general treatment of higher order modes (assuming flat beams). Below, we will mention the analysis of Ref. 58 as an illustration of the technique. To proceed, let the beam distributions be written as infinitesimal perturbations on top of a steady-state Ψ_0 as Eq. (1). The Vlasov equation is then linearize in $\Delta\Psi_\pm$ and the resultant equations are transformed from the Cartesian variables (y, y') to the action-angle variables (J, ϕ). The beam-beam force is localized in this analysis.

The problem becomes soluble if we assume a water-bag model of the unperturbed steady-state distribution

$$\Psi_0 = (1/\pi\varepsilon)\, H(\varepsilon/2 - J) \tag{37}$$

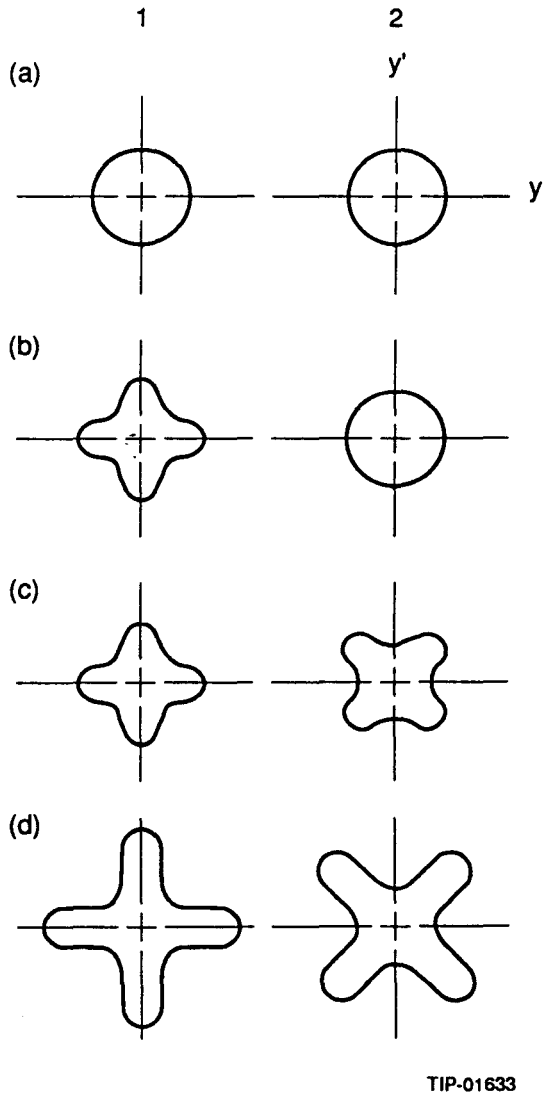

Figure 22. Coherent Beam-beam Octupole Mode Instability.

where ε is the unperturbed beam emittance; $H(x) = 1$ if $x > 0$ and 0 if $x < 0$.

The choice of water-bag model makes the solution of the problem particularly simple, but this is not without cost. The imposed distribution Eq. (37) is inconsistent with the steady-state condition, Eqs. (15) - (16). The problem is therefore solved but not self-consistently.

Coherent beam-beam instability is pronounced near resonances

$$\nu = 2\nu_0 \approx m/n \tag{38}$$

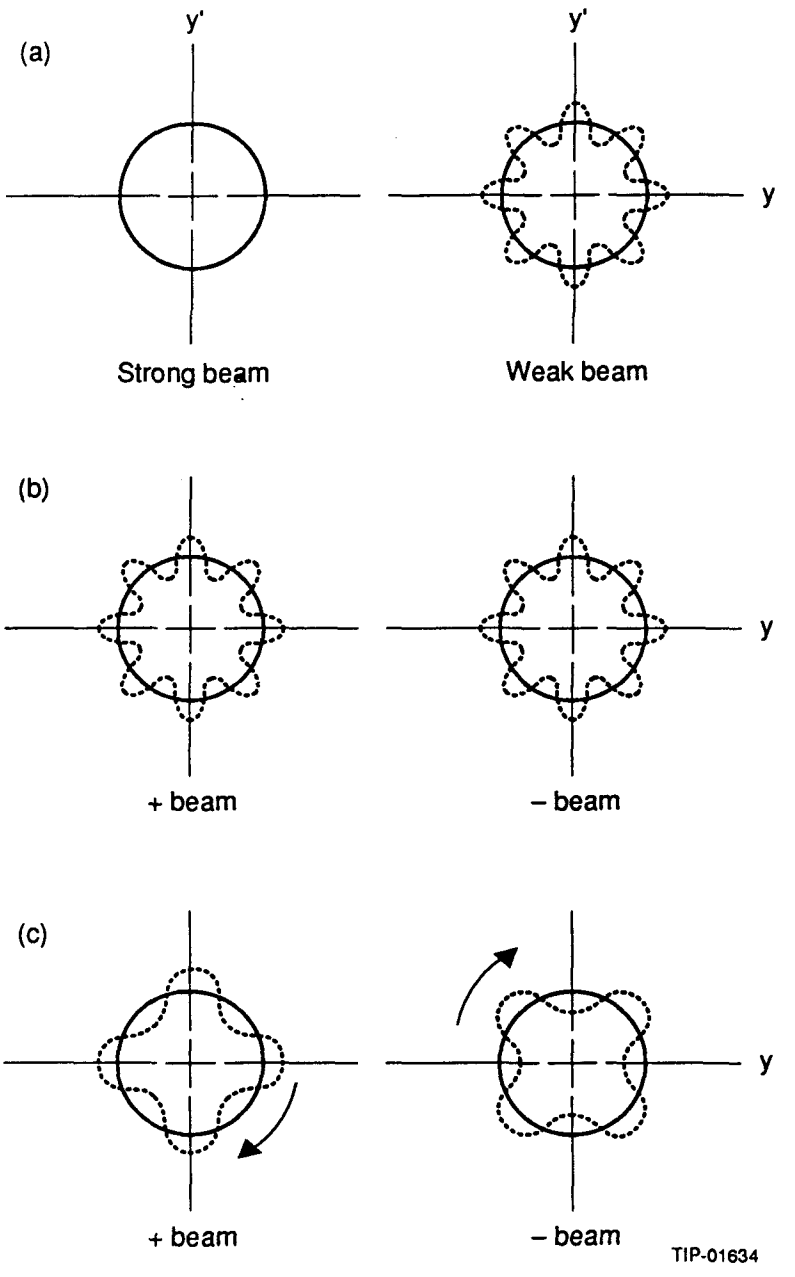

Figure 23. Beam Behavior in Phase Space of Two Beams for (a) Incoherent Strong-weak Case, (b) Dynamic-beta Effect, (c) One of the Coherent Octupole Modes; (b) and (c) are Strong-strong Cases. The solid and dashed curves indicate the unperturbed and the beam-beam perturbed distributions, respectively. The perturbed distribution moves with time in (c) but is static in (a) and (b).

in which case the most perturbed mode is the n-th mode ($n = 1, 2, 3\ldots$ for dipole, quadrupole, sextupole... modes, respectively),

$$\Delta\Psi \sim \exp(\mathrm{i}n\phi)\,. \tag{39}$$

For the water-bag model, the perturbed mode frequency is given by[58]

$$\cos\mu = \cos(2\pi n\nu) \pm \frac{8n}{4n^2-1}\,\zeta\sin(2\pi n\nu) \tag{40}$$

where $\pm$ refer to the in-phase or out-of-phase mode patterns (the 0- and the π-modes). Instability results from having $|\cos\mu| > 1$, which occurs when $|\cos(2\pi n\nu)|$ is close to unity, or when Eq. (38) is satisfied. Around the resonance (38), there is a stopband within which the beams are unstable. From Eq. (40), one obtains the stopband width around the resonance:

$$\delta\nu_n = \frac{\zeta}{2\pi}\,\frac{16}{4n^2-1}\,. \tag{41}$$

Figure 24 is the sawtooth diagram for 2 bunches per beam. As more and more modes are included, higher and higher order resonances become involved. When the maximum mode number is n, resonances up to order n near $\nu = m/n$ are excited. Figure 25 shows the dependence of the sawtooth diagram on the number of bunches. The higher order resonance behavior can be rather complex.

In analogy to single-particle nonlinear dynamics, the Chirikov criterion may be applied by summing the stopband widths of all resonances. The total width is $\Sigma n\delta\nu_n$ which diverges if Eq. (41) is used. This means that, for the water-bag model, no region in tune space is free of resonance effects. However, the water-bag model does not provide any tune dependence with amplitude because all dynamics occur at one amplitude only, namely the amplitude corresponding to the edge of the bag. This means there is no consideration of Landau damping effects, which is a deficiency of the water-bag model.

It is important to keep in mind one special feature of the beam-beam interaction. Unlike nonlinear fields due to magnet imperfections, the beam-beam effect is intrinsically stable in the sense that it perturbs only particles in the beam core and not particles with large amplitudes. As a core particle becomes unstable, it necessarily grows out of the instability as its amplitude increases. This detuning effect plays an important role in determining the characteristics of the incoherent beam-beam effects. The same physical feature will also play an important role in the coherent beam-beam effects by manifesting itself through

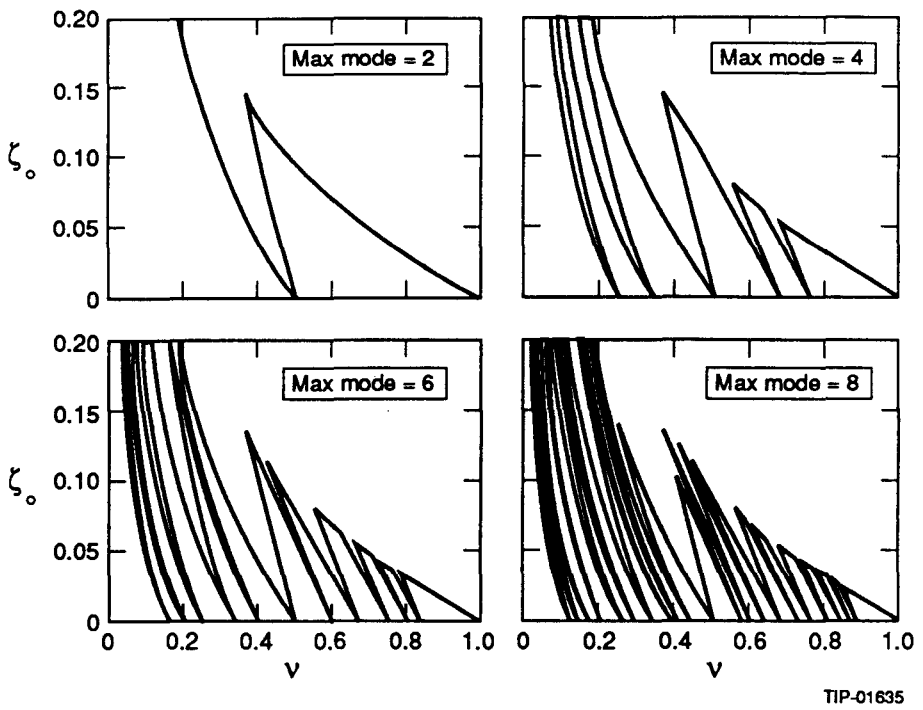

Figure 24. Sawtooth Diagrams for the Case of $M = 2$ and Varying Maximum Mode Number $= 2, 4, 6,$ and 8.

Landau damping. A complete analysis of coherent beam-beam effects will have to consider Landau damping effects. When Landau damping is included, the difference between coherent and incoherent effects blurs.

Higher order modes can also be studied by numerical simulations. Although not emphasized in this review, a remark is to be made consistent with previous discussions. To study the coherent beam-beam effects, it is important in the simulation to allow the beam distribution to deviate from gaussian so that higher order modes are allowed to grow. Restricting the beam distribution to gaussian shape is equivalent to simulating each beam by two macro-particles even when a thousand particles are used. The approach of allowing for nongaussian distortions has been taken by the more recent simulation codes.[63–66]

10.0 COHERENT BEAM BLOW-UP MODEL

The coherent beam-beam instability provides a possible description of the observed beam-beam limit.[67] For a given choice of tune away from resonances, consider the situation as the beam intensity N is increased from zero. At first, the beams are stable, beam sizes are given by their unperturbed values, beam-beam parameter is proportional to N, and

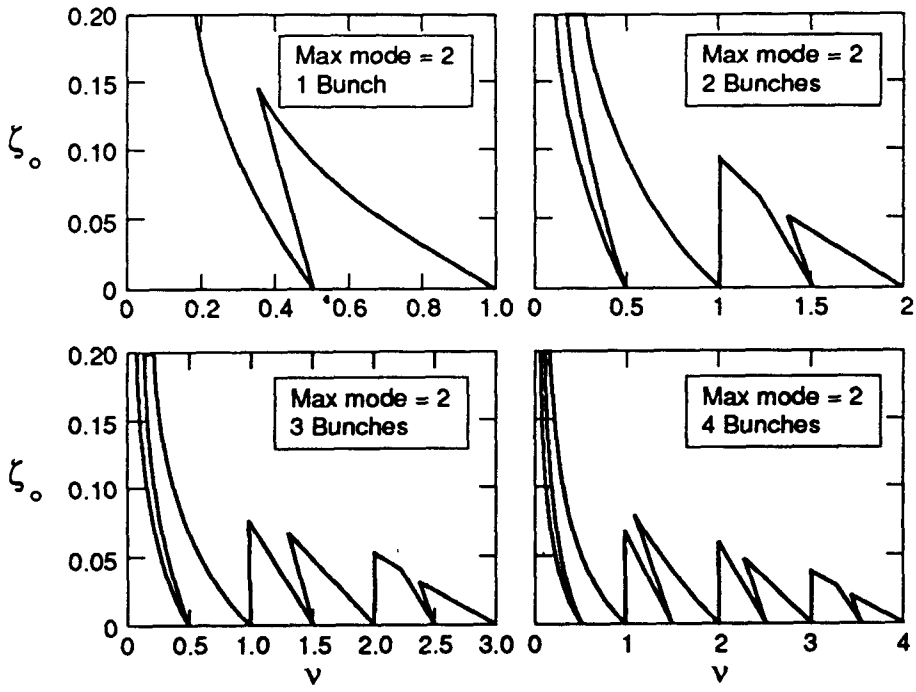

(a)

Figure 25. Sawtooth Diagrams for Different Number of Bunches $M = 1, 2, 3, 4$; (a), (b) and (c) are Three Sets for Varying Maximum Mode Number $= 2, 3$ and 4, Respectively.

luminosity is proportional to N^2. As N is increased to reach the boundary of the sawtooth curve, the beams become unstable, the beam sizes grow. However, they grow only by so much as to make ζ stay just under the sawtooth curve. In other words, as N is increased beyond a certain threshold, ζ is saturated at a certain critical value (the beam-beam limit). The beam size and the luminosity then behave as shown in Figure 26 for the flat- and round-beam cases.

This coherent blow-up model is analogous to the bunch lengthening phenomenon observed in electron storage rings. Observe that a similar situation has been encountered when the dynamic-beta effect was discussed, in which the beams continue to blow up as N is increased in such a way that instability (4) is always avoided.

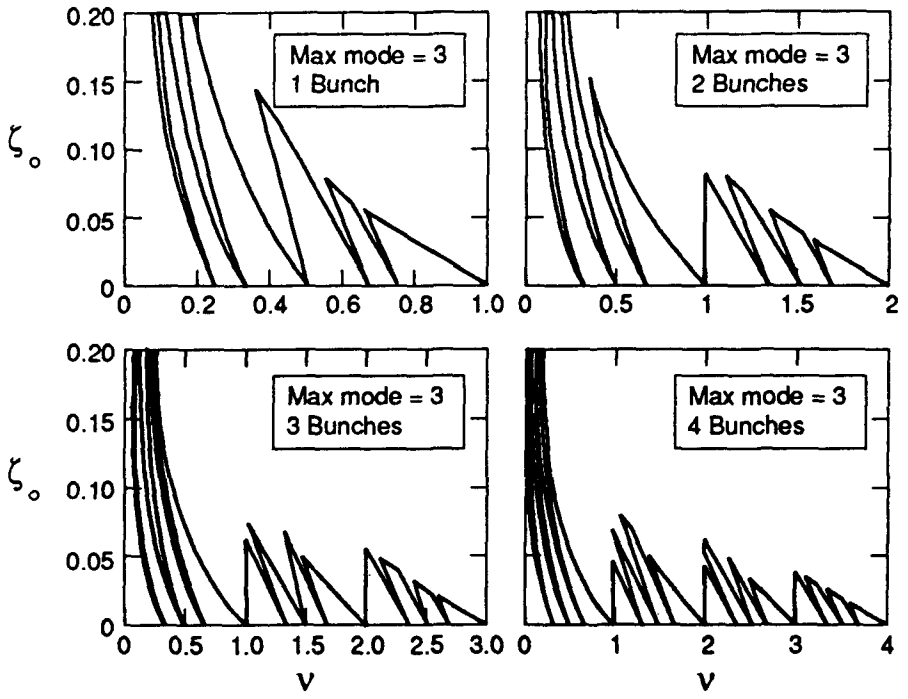

(b)

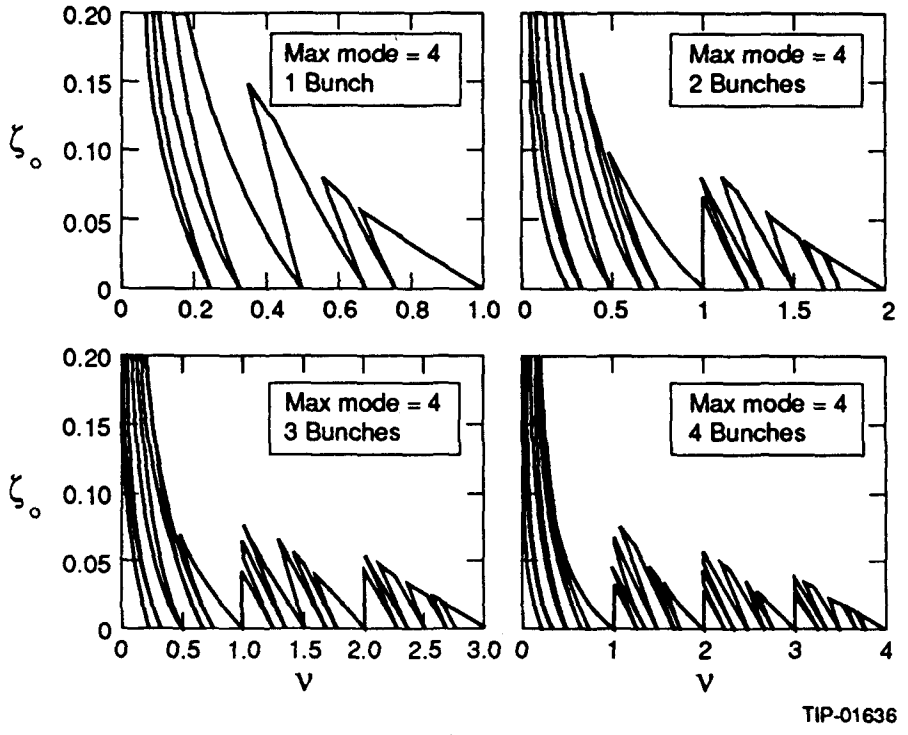

(c)

Figure 25 (Continued)

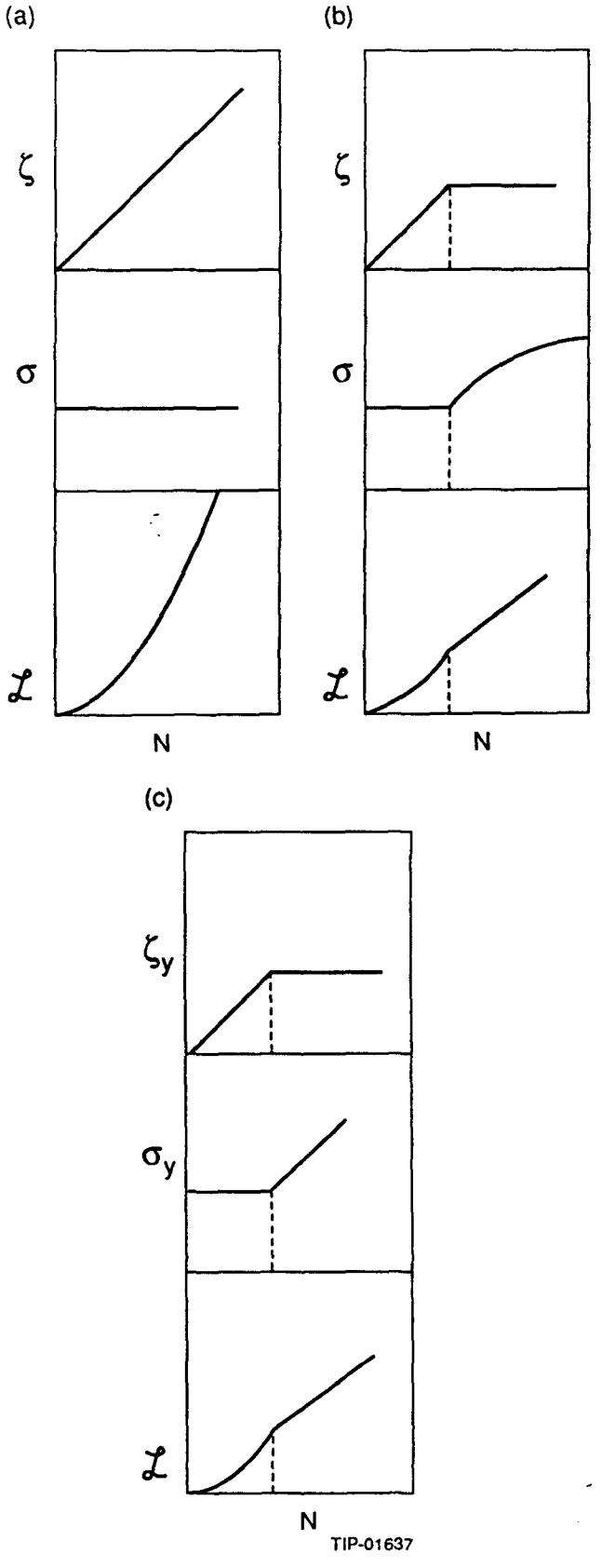

Figure 26. Behavior of Beam-beam Parameter, Beam Size and Luminosity as Functions of Beam Intensity for Three Cases: (a) Unperturbed, (b) Round Beams, (c) Flat Beams. Dotted lines indicated a beam-beam threshold.

REFERENCES

1. See, for example, *Nonlinear Dynamics and the Beam-beam Interaction, BNL*, AIP Proc. No. 57, M. Month and J.C. Herrera, eds., 1979.
2. B. Richter, Proc. Int. Symp. Electron and Positron Storage Rings, Saclay, 1966, p. I-1-1.
3. M.H.R. Donald and J.M. Paterson, *An Investigation of the Flip-flop Beam-beam Effect in SPEAR*, IEEE Trans. Nuc. Sci. **NS-26**, 3580 (1979).
4. H. Wiedemann, *Experiments on the Beam-beam Effect in e+e− Storage Rings*, AIP Proc. No. 57, M. Month and J.C. Herrera, eds., 84 (1979).
5. J.F. Tennyson, *Flip-flop Modes in Symmetric and Asymmetric Colliding-beam Storage Rings*, LBL-28013 (1989).
6. J.F. Tennyson, lectures at this school.
7. S. Kheifets and A.W. Chao, *Steady-state Distribution for Unbunched Beams Colliding in a Drift Space*, SLAC report PEP-325 (1979).
8. A. Piwinski, *Coherent Beam Break-Up Due to Space Charge*, Proc. 8-th Int. Conf. High Energy Accel., CERN, 357 (1971).
9. A. Chao and E. Keil, *Coherent Beam-beam Effect*, CERN/ISR-TH/79-31 or SLAC report PEP-300 (1979).
10. E. Keil, *Coherent Beam-beam Effect in LEP*, CERN report LEP-178, (1979).
11. E. Keil, *Visible Frequencies in the Coherent Beam-beam Effect With More Than One Bunch in Each Beam*, CERN report LEP-268 (1980).
12. E. Keil, *Theoretical Aspects of the Beam-beam Interaction*, Proc. 11-th Int. Conf. High Energy Accel., CERN, 759 (1980).
13. E. Keil, *Visible Frequencies in the Nonlinear Coherent Beam-beam Effect*, CERN report LEP-294 (1981).
14. E. Keil, *Nonlinear Coherent Effects Between Two Strong Bunched Beams Colliding in a storage Ring*, Nucl. Instr. Meth. **188**, 9 (1981).
15. J.D. Bjorken, Workshop on p-pbar Options for the Super Collider, U. Chicago, Fermilab Conf.-84/29-THY (1984).
16. R. Talman, *Multiparticle Phenomena and Landau Damping*, AIP Proc. 153, Accelerator Summer School, SLAC and Fermilab, 789 (1987).

17. A. Hofmann and S. Myers, *Evaluation of the Absolute LEP Luminosity from Measurement of the Coherent Beam-beam Tune Split*, CERN report LEP-604, (1988).

18. K. Hirata, *Coherent Betatron Oscillation Modes Due to Beam-beam Interaction*, Nucl. Instr. Meth. Phys. Res. **A269**, 7 (1988).

19. K. Yokoya, Y. Funakoshi, E. Kikutani, H. Koiso and J. Urakawa, KEK Preprint 89-14 (1989).

20. E. Keil, *Four Beam Compensation Schemes*, CERN LEP-TH/89-37, 3rd Advanced ICFA Beam Dynamics Workshop on Beam-beam Effects in Circular Colliders, Novosibirsk, 85 (1989).

21. SPEAR Group, *Beam-Beam Coupling in SPEAR*, Proc. 9th Int. Conf. High Energy Accel., Stanford, 1974, p.66.

22. A. Piwinski, *Recent Results from DORIS and PETRA*, AIP Proc. No. 57, M. Month and J.C. Herrera, eds., 1979.

23. A. Piwinski, *Observation of Beam-beam Effects in PETRA*, IEEE Trans. Nucl. Sci. **NS-26**, 4268 (1979).

24. T. Ieiri, T. Kawamoto and K. Hirata, Nucl. Instru. Meth. Phys. Res. **A265**, 364 (1988).

25. K. Satoh, Proc. 6th Symp. Accel. Tech., Tokyo, 1987, p.18.

26. T. Ieiri and K. Hirata, *Observation and Simulation of Nonlinear Behavior of Betatron Oscillations During the Beam-beam Collision*, Proc. IEEE Part. Accel. Conf., Chicago, 709 (1989).

27. For a review of coherent dipole and quadrupole effects, see K. Hirata, *The Beam-beam Interaction: Coherent Effects*, AIP Proc. 214, Workshop on Beam Dynamics Issues of High Luminosity Asymmetric Colliders, LBL, 175 (1990).

28. E. Keil, *Coherent Beam-beam Effects in Machines with Unequal Betatron Phase Advances Between Crossing Points*, CERN report LEP-226 (1980).

29. K. Hirata and E. Keil, *Barycentre Motion of Beams Due to Beam-beam Interaction in Asymmetric Ring Colliders*, CERN/LEP-TH/89-76 (1989).

30. K. Hirata and E. Keil, *Coherent Beam-beam Interaction Limit in Asymmetric Ring Colliders*, Phys. Lett. **B232**, 413 (1989).

31. Y. Kamiya and A.W. Chao, *Coherent Synchro-betatron Oscillations Excited by the Beam-beam Interaction*, SLAC/AP-10 (1983).

32. K. Hirata, *Barycenter Motion of Beams Under the Beam-beam Interaction*, KEK report TN-880010 (1989).

33. M. Furman and A. Chao, *Effect of Long Range Beam-beam Interaction on the Stability of Coherent Dipole Motion*, IEEE Trans. Nucl. Sci. **NS-32**, 2297 (1985).

34. E. Forest, *Treatment of the Long Range Coherent Beam-beam with the Vlasov Equation*, SSC-51 (1986).

35. K. Hirata, *The Long Range Beam-beam Force: Effects on the B Factory*, AIP Proc. 214, Workshop on Beam Dynamics Issues of High Luminosity Asymmetric Colliders, LBL, 441 (1990).

36. E. Forest and M. Furman, *Algebraic Theory of Beam-beam Interaction in the Thin Lens Model*, SSC-32, (1985).

37. M.A. Furman, *Results of Coherent Dipole Beam-beam Interaction Studies for SSC Lattices*, SSC-62, (1986).

38. J.E. Augustin et al., Proc. 7-th Int. Conf. High Energy Accel., Yerevan, Vol. 2, 113 (1970).

39. G. Arzelier et al., Proc. 8-th Int. Conf. High Energy Accel., CERN, 150 (1971).

40. N.N. Chau and D. Potaux, *Stabilite des Oscillations Transverses dans un Anneau a Charge D'Espace Compensee, I. Methode de Calcul*, Orsay Tech. Report 5-74 (1974).

41. N.N. Chau and D. Potaux, *Stabilite des Oscillations Transverses dans un Anneau a Charge D'Espace Compensee, II. Application au Choix d'un Point de Fonctionnement*, Orsay Tech. Report 2-75 (1975).

42. Ya.S. Derbenev, Proc. III All Union Part. Accel. Conf., Moscow, 382 (1973).

43. Ya.S. Derbenev, *Collective Instability of Compensated Colliding Beams*, SLAC TRANS-151 (1973).

44. N.S. Dikansky and D.V. Pestrikov, *Colliding Beams Coherent Instability*, Part. Accel. **12**, 27 (1982).

45. Ya.S. Derbenev, N.S. Dikansky, D.V. Pestrikov, Preprint 7-75, INPh, Siberian Division, USSR Academy of Sciences, 1972.

46. A.W. Chao, *The Beam-beam Instability*, AIP Proc. 127, Accel. Summer School, BNL/SUNY, M. Month, P. Dahl, and M. Dienes, eds., 201 (1983).

47. Y. Kamiya and A. Chao, *Stability of the Coherent Quadrupole Oscillations Excited by the Beam-beam Interaction*, SLAC/AP-8 (1983).

48. Historically the second model was introduced before the first model. The order has been reversed below to simplify the discussions.

49. M.A. Furman, K.Y. Ng and A.W. Chao, *A Symplectic Model of Coherent Beam-beam Quadrupole Modes*, SSC-174 (1988).

50. M.A. Furman, *A Symplectic Coherent Beam-beam Model*, 3rd Advanced Beam Dynamics Workshop on Beam-beam Effects in Circular Colliders, Novosibirsk, 52 (1989).

51. K.Y. Ng, *Linear Beam-beam Effects for Round Beams*, SSC-161, (1988).

52. K. Hirata, *Solvable Model of the Beam-beam Limit in e+e− Colliding Rings*, Phys. Rev. Lett. **58**, 25 (1987); **58**, 1798(E) (1987).

53. K. Hirata, *Solvable Model, Flip-flop Hysteresis and Catastrophe in e+e− Colliding Storage Rings*, KEK-Preprint 86-102 (1987).

54. K. Hirata, *Solvable Model of Beam-beam Effects in e+e− Colliding Storage Rings*, Phys. Rev. **D37**, 1307 (1988).

55. H.S. Uhm and C.S. Liu, *Filamentation Instability of Electron and Positron Colliding Beams in Storage Ring*, Phys. Rev. Lett. **43**, 914 (1979).

56. B. Zotter, *Filamentation Instability in LEP*, CERN Report LEP-194, (1979).

57. R.E. Meller and R.H. Siemann, *Coherent Normal Modes of Colliding Beams*, IEEE Trans. Nucl. Sci., **NS-28**, 2431 (1981).

58. A.W. Chao and R.D. Ruth, *Coherent Beam-beam Instability in Colliding-beam Storage Rings*, Part. Accel. **16**, 201 (1985).

59. E. Forest, *A Theory of Coherent Beam-beam Effects with Long-range Interactions*, Part. Accel. **21**, 133 (1987).

60. K. Hirata, *Beyond Gaussian Approximation for Beam-beam Interaction—an Attempt*, CERN/LEP-TH/88-56 (1988).

61. N.S. Dikansky and D.V. Pestrikov, *Collective Beam-beam Phenomena*, 3rd Advanced Beam Dynamics Workshop on Beam-beam Effects in Circular Colliders, Novosibirsk, 76 (1989).

62. K. Hirata, *Stratonovich Expansion and Beam-beam Interaction*, CERN/LEP-TH/89-14 (1989).

63. K. Hirata and E. Keil, *A Program for Computing Beam-beam Modes*, CERN/LEP-TH/89-57 (1989).

64. S. Krishnagopal, Ph.D. thesis, Cornell University, 1990.

65. J. Koga, Ph.D. thesis, University of Texas at Austin, 1990.

66. A. Chao, M. Furman, N.K. Mahale, R. Siemann, S. Krishnagopal, T. Tajima, J. Koga, *Summary Report of the Mini-workshop on Beam-beam Simulations*, SSC-N-702, (1990).

67. A.W. Chao, P. Bambade and W.T. Weng, *Nonlinear Beam-beam Resonances*, Lecture Notes in Phys. 247, Springer-Verlag, J.M. Jowett, M. Month and S. Turner, eds., 77 (1985).